Supporting Information

to

Multifunctional SAHA-Derived 8-Hydroxyquinoline Metallopharmacophores: HDAC Inhibition and Antiproliferative Activity

Chen Chen, [a] Barbora Havlínová, [b] Miroslava Vošahlíková, [b] Růžena Tučková, [b] Julia Stjärnhage, [a] Zexiong Lin, [a] Charlotte Rayner, [a] Cyril Bařinka, [b] Tilo Söhnel, [a] Stephen M. F. Jamieson, [c] and Christian G. Hartinger*[a]

[a] *School of Chemical Sciences, University of Auckland, Private Bag 92019, Auckland, New Zealand.*
[b] *Institute of Biotechnology of the Czech Academy of Sciences, BIOCEV, Vestec, Czech Republic.*
[c] *Auckland Cancer Society Research Centre, University of Auckland, Auckland, New Zealand*

Table of Contents

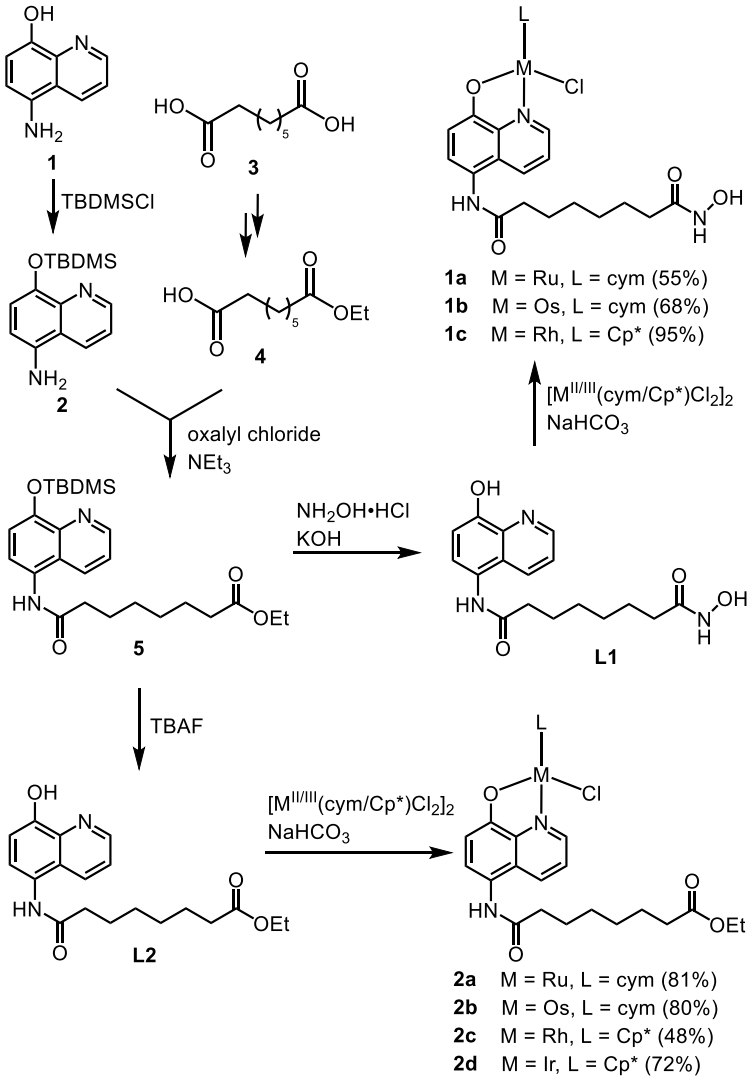

Scheme S1. Preparation of metal complexes **1a**–**1c** and **2a**–**2d** from 5-amino-8-hydroxyquinoline.

Experimental procedures

Materials and methods

All air-sensitive reactions were carried out under nitrogen atmosphere in standard Schlenk flasks. Chemicals and solvents purchased from commercial suppliers were used without further purification. All synthesised reagents were dried under vacuum in Schlenk flasks prior to elemental analyses and their use in biological assays. α-Terpinene (89%), sodium sulfide nonahydrate (≥ 98.0%), suberic acid (AK Scientific), HCl (Loba Chemie, 37%), $NH_2OH{\cdot}HCl$ ((AK Scientific, 98%), 5-aminoquinolin-8-ol (Combi-Blocks, Inc.), foetal bovine serum (ThermoFisher Scientific), foetal calf serum (Moregate Biotech), oxalyl chloride (Merck Life Science Ltd, 98%), α-MEM (Life Technologies), $OsCl_3{\cdot}xH_2O$ (Heraeus South Africa, 55% metal content), pentamethylcyclopentadiene (Sigma-Aldrich, 95%), $RuCl_3{\cdot}xH_2O$, $RhCl_3{\cdot}xH_2O$ and $IrCl_3{\cdot}xH_2O$ (Precious Metals Online, 99%), $AgNO_3$ (ECP), $NaHCO_3$ (ECP, analytical reagent), NaOH (BDH Chemicals, analytical reagent), sulforhodamine B sodium salt (AK Scientific, technical grade), Cisplatin (AK Scientific, 95%) and α-terpinene (Sigma-Aldrich, ≥89%) were obtained from commercial sources. 8-((tert-Butyldimethylsilyl)oxy)quinolin-5-amine **2**,[1] 8-ethoxy-8-oxooctanoic acid **4**,[2, 3] and dimeric precursors bis[dichlorido(η^6-*p*-cymene)ruthenium(II)],[4] bis[dichlorido(η^6-*p*-cymene)osmium(II)],[4] bis[dichlorido(η^5-pentamethylcyclopentadienyl)iridium(III)],[5] bis[dichlorido(η^5-pentamethylcyclopentadienyl)rhodium(III)],[5] 8-((tert-butyldimethylsilyl)oxy)quinolin-5-amine,[1] and 8-ethoxy-8-oxooctanoic acid[6] were prepared as described in the literature. Water (18.2 MΩ) used throughout these experiments was obtained from a Millipore Milli-Q Gradient Water Purification System. PBS used throughout the cell culture experiments was prepared in the lab using NaCl, KCl, KH_2PO_4 anhydrous and Na_2HPO_4 purchased from Merck.

NMR spectra were recorded on Bruker AV300 or Bruker DRX 400 MHz NMR spectrometers at ambient temperature at 300.13 MHz/399.89 MHz (^{1}H), 100.61 MHz (^{13}C{^{1}H}, ^{13}C{^{1}H} DEPT-Q), with chemical shifts (δ in ppm) reported relative to the residual solvent peaks of the deuterated solvents. $CDCl_3$ and DMSO-d_6, MeOD-d_4, and D_2O were used as NMR solvents. Mass spectrometry (MS) data were recorded on either Bruker microOTOF-QII or ThermoScientific Orbitrap Exploris 120 mass spectrometers in positive electrospray ionisation (ESI) mode at the Mass Spectrometry Centre, The University of Auckland. Elemental analyses were conducted on a vario EL cube (Elementar Analysensysteme GmbH, Hanau, Germany) using CHN mode for ligands, and complexes containing Ru, Rh, and Ir. Elemental analyses for the Os complexes **1b** and **2b** were carried out on a vario MICRO (Elementar Analysensysteme GmbH) at Macquarie University Chemical Analysis and Biotechnology Centre (MUCAB).

For ICP-MS sample preparation, nitric acid (HNO_3, 69% Suprapure, Merck), Ru standard solution (1000 ± 5 μg/mL, Inorganic Ventures), Os standard solution (1000 ± 10 μg/mL, Inorganic Ventures), Pt

standard solution (1000 µg/mL, CPI International) and Rh elemental standard (1000 mg/L, Centipur, Merck KGaA) were used.

Synthesis

Ethyl 8-((8-((tert-butyldimethylsilyl)oxy)quinolin-5-yl)amino)-8-oxooctanoate ***5***

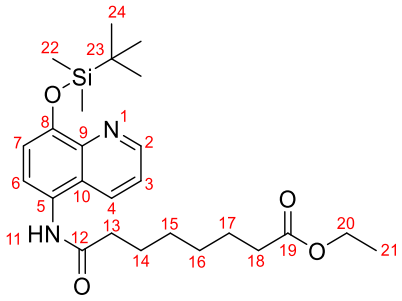

5

Adapted from a procedure by Chalmers *et al*,[6] 8-ethoxy-8-oxooctanoic acid **4** (1.52 g, 7.50 mmol) was dissolved in anhydrous DCM (35 mL) at room temperature under N_2 atmosphere. Oxalyl chloride (1.28 mL, 15 mmol) and anhydrous DMF (1 drop) were added, and the solution was left to stir for 2 h. DCM was removed *in vacuo* to give ethyl 8-chloro-8-oxooctanoate. The acid chloride was dissolved in anhydrous DCM (20 mL) under N_2. 8-((tert-Butyldimethylsilyl)oxy)quinolin-5-amine **2** (1.37 g, 5.00 mmol) and triethylamine (1.38 mL, 10.0 mmol) were suspended in anhydrous DCM (35 mL) under N_2 and cooled to 0 °C. A solution of ethyl 8-chloro-8-oxooctanoate in DCM (35 mL) was added dropwise under stirring and the solution was stirred for 15 min afterwards. After the consumption of 8-((tert-butyldimethylsilyl)oxy)quinolin-5-amine, as monitored by TLC, DCM was removed *in vacuo* and the residue isolated by column chromatography (hexanes:EtOAc 4:1 v/v) to give crude compound **5** as an orange solid. The compound was used without further purification for the synthesis of **L1** and **L2**.

N^1-hydroxy-N^8-(8-hydroxyquinolin-5-yl)octanediamide ***L1***

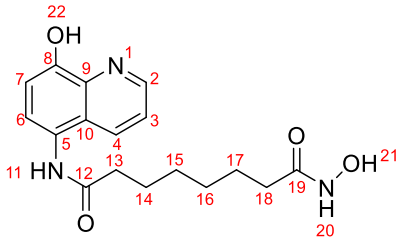

L1

Adapted from a procedure by Chalmers *et al*,[6] a solution of KOH (5.40 g, 100 mmol) in MeOH (30 mL) was added slowly to a stirred solution of hydroxylamine hydrochloride (3.45 g, 50 mmol) in MeOH (30 mL) at 0 °C. The solution was stirred for 30 min. A solution of compound **5** (2.29 g, 5 mmol) in MeOH (30 mL) was added dropwise under N_2 at 0 °C and the solution was allowed to stir overnight. MeOH was removed *in vacuo* and water (50 mL) was added followed by slow addition of 1 M HCl until pH 5 was reached. The resultant white precipitate was filtered, dried, and recrystallised from

MeOH to obtain **L1** as a white solid (1.08 g, 65%). HRMS (ESI$^+$): *m/z* 332.1607 $[M + H]^+$ (m_{calc} = 332.1605). EA calculated for $C_{17}H_{21}N_3O_4$: C 61.62, H 6.39, N 12.68%; found: C 61.42, H 6.30, N 12.61%. ^{1}H NMR (400 MHz, DMSO-d_6) δ (ppm) 10.33 (s, 1H, H-20), 9.70 (s, 2H, H-11/22), 8.86 (dd, *J* = 4.1, 1.6 Hz, 1H, H-2), 8.65 (s, 1H, H-21), 8.28 (dd, *J* = 8.6, 1.6 Hz, 1H, H-4), 7.59 (dd, *J* = 8.6, 4.1 Hz, 1H, H-3), 7.42 (d, *J* = Hz, 1H, H-6), 7.05 (d, *J* = 8.2 Hz, 1H, H-7), 2.40 (t, *J* = 7.4 Hz, 2H, H-13), 1.96 (t, *J* = 7.4 Hz, 2H, H-18), 1.70–1.58 (m, 2H, H-14), 1.58–1.46 (m, 2H, H-17), 1.41–1.25 (m, 4H, H-15/16). ^{13}C{^{1}H} NMR (101 MHz, DMSO-d_6) δ (ppm) 174.32 (C-12), 171.04 (C-19), 152.02 (C-8), 149.21 (C-2), 138.92 (C-9), 132.69 (C-4), 125.61 (C-6), 125.55 (C-10), 124.93 (C-5), 122.55 (C-3), 111.30 (C-7), 36.37 (C-13), 32.97 (C-18), 29.05 (C-14), 28.92 (C-17), 25.99 (C-15), 25.74 (C-16).

Ethyl 8-((8-hydroxyquinolin-5-yl)amino)-8-oxooctanoate ***L2***

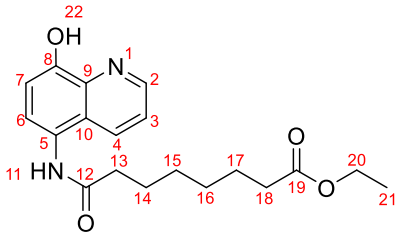

L2

A solution of TBAF in THF (7.5 mL, 1 M) was added dropwise to a solution of compound **5** (2.29 g, 5.0 mmol) in THF (50 mL) at 0 °C. The reaction progress was monitored by ^{1}H NMR spectroscopy and completed after 3 h. HOAc (429 µM, 7.5 mmol) was then added, followed by quenching with water. After THF evaporation, the resulting precipitate was filtered and washed with water. The crude product was suspended in i-PrOH and stirred overnight. Filtration and washing with i-PrOH yielded **L2** as a white solid (0.90 g, 53%). HRMS (ESI$^+$): *m/z* 345.1808 $[M + H]^+$ (m_{calc} = 345.1809). EA calculated for $C_{19}H_{24}N_2O_4$: C 66.26, H 7.02, N 8.13%; found: C 66.08, H 7.12, N 8.07%. ^{1}H NMR (400 MHz, DMSO-d_6) δ (ppm) 9.71 (s, 2H, H-11), 8.86 (dd, *J* = 4.1, 1.5 Hz, 1H, H-2), 8.29 (dd, *J* = 8.6, 1.6 Hz, 1H, H-4), 7.58 (dd, *J* = 8.6, 4.1 Hz, 1H, H-3), 7.43 (d, *J* = 8.2 Hz, 1H, H-6), 7.05 (d, *J* = 8.2 Hz, 1H, H-7), 4.05 (q, *J* = 7.1 Hz, 2H, H-20), 2.41 (t, *J* = 7.4 Hz, 2H, H-13), 2.29 (t, *J* = 7.4 Hz, 2H, H-18), 1.70 – 1.60 (m, 2H, H-14), 1.60 – 1.49 (m, 2H, H-17), 1.42 – 1.29 (m, 4H, H-15, 16), 1.17 (t, *J* = 7.1 Hz, 3H, H-21). ^{13}C{^{1}H}DEPT-Q (101 MHz, DMSO-d_6) δ (ppm) 172.87 (C-19), 172.05 (C-12), 151.23 (C-5), 148.00 (C-2), 138.27 (C-9), 132.02 (C-4), 124.50 (C-10), 124.48 (C-8), 124.13 (C-6), 121.39 (C-3), 110.38 (C-7), 59.64 (C-20), 35.62 (C-13), 33.48 (C-18), 28.41 (C-15/16), 28.22 (C-15/16), 25.16 (C-14), 24.37 (C-17), 14.12 (C-21).

General procedure*: Synthesis of mononuclear 8-hydroxyquinoline complexes* ***1a−1c****, and* ***2a−2d****.*
Sodium bicarbonate (1.1 equiv.) was added to a dry MeOH/DCM (1:1) solution of **L1** or **L2** (1 equiv.) under a nitrogen atmosphere at room temperature and the reaction mixture was stirred for 10 min. Then, $[M^{II/III}(cym/Cp^*)Cl_2]_2$ (0.5 equiv.; M^{II} = Ru/Os, M^{III} = Rh/Ir) was added, and the reaction was stirred at

35 °C for 5 h under nitrogen. After cooling to room temperature, the mixture was filtered through Celite and washed with MeOH and DCM mixture. Then the solvent was removed under reduced pressure, and the complex was precipitated with DCM and diethyl ether. The precipitate was collected by filtration, washed with Et_2O, and dried *in vacuo* to give pure products, as determined by elemental analysis.

Chlorido(N^{20}-hydroxy-N^{11}-(8-hydroxyquinolin-5-yl)octanediamide-κ^2N,O)(η^6-p-cymene)ruthenium(II) ***1a***

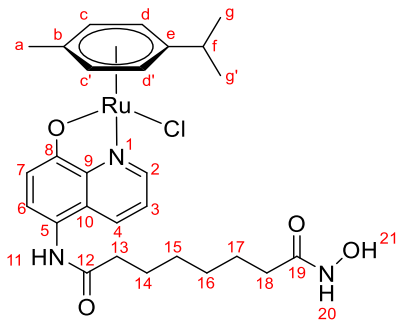

1a

The synthesis was performed according to the general procedure using **L1** (166 mg, 0.50 mmol), $NaHCO_3$ (46 mg, 0.55 mmol), and $[Ru(cym)Cl_2]_2$ (153 mg, 0.25 mmol) to afford **1a** as a brown solid (164 mg, 55%). HRMS (ESI^+): *m/z* 566.1594 $[M - Cl]^+$ (m_{calc} = 566.1595). EA calculated for $C_{27}H_{34}ClN_3O_4Ru \cdot 2H_2O$: C 50.90, H 6.01, N 6.60%; found: C 51.10, H 5.77, N 6.57%. ^1H NMR (400 MHz, DMSO-d_6) δ (ppm) 10.33 (s, 1H, H-20), 9.45 (s, 1H, H-11), 9.20 (d, J = 4.2 Hz, 1H, H-2), 8.65 (s, 1H, H-21), 8.06 (d, J = 8.3 Hz, 1H, H-4), 7.52 (dd, J = 8.1, 4.9 Hz, 1H, H-3), 7.12 (d, J = 8.2 Hz, 1H, H-6), 6.62 (d, J = 8.3 Hz, 1H, H-7), 5.85 – 5.76 (m, 2H, H-d, d'), 5.61 – 5.50 (m, 2H, H-c, c'), 2.74–2.61 (m, 1H, H-f), 2.33 (t, J = 6.9 Hz, 2H, H-13), 2.14 (s, 2H, H-a), 1.95 (t, J = 6.8 Hz, 2H, H-18), 1.67–1.56 (m, 2H, H-14), 1.56–1.46 (m, 2H, H-17), 1.40–1.25 (m, 4H, H-15/16), 1.11 – 1.01 (m, 6H, H-g, g'). ^{13}C NMR (101 MHz, DMSO-d_6) δ (ppm) 172.18 (C-12), 169.23(C-19), 167.19 (C-8), 149.82 (C-2), 143.56 (C-9), 133.47 (C-4), 126.84 (C-6), 125.53 (C-10), 122.06 (C-3), 117.17 (C-5), 111.50 (C-7), 100.02 (C-e), 98.00 (C-b), 82.45 (C- d/d'), 81.78 (C- d/d'), 80.51 (C-c'), 80.14 (C-c), 35.57 (C-13), 32.30 (C-18), 30.44 (C-f), 28.54 (C-15), 28.43 (C-16), 25.35 (C-14), 25.11 (C-17), 22.00 (C-g/g'), 21.81 (C-g/g'), 18.13 (C-a).

Chlorido(N^{20}-hydroxy-N^{11}-(8-hydroxyquinolin-5-yl)octanediamide-κ^2N,O)(η^6-p-cymene)osmium(II) ***1b***

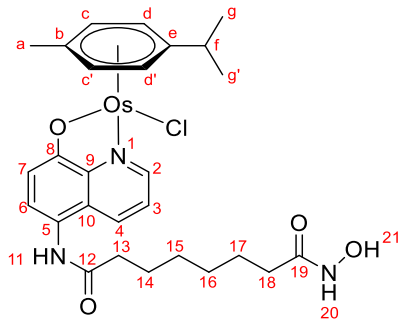

1b

The synthesis was performed according to the general procedure using **L1** (166 mg, 0.50 mmol), $NaHCO_3$ (46 mg, 0.55 mmol), and $[Os(cym)Cl_2]_2$ (201 mg, 0.25 mmol) to afford **1b** as a yellow solid (234 mg, 68%). HRMS (ESI^+): *m/z* 640.2216 $[M - Cl - OH + H]^+$ (m_{calc} = 640.2211). EA calculated for $C_{27}H_{34}ClN_3O_4Os \cdot 1.5H_2O$: C 45.21, H 5.20, N 5.86%; found: C 45.18, H 4.95, N 5.81%. ^1H NMR (400 MHz, DMSO-d_6) δ (ppm) 10.34 (s, 1H, H-20), 9.54 (s, 1H, H-11), 9.09 (d, J = 4.7 Hz, 1H, H-2), 8.65 (s, 1H, H-21), 8.06 (d, J = 8.4 Hz, 1H, H-4), 7.49 (dd, J = 8.5, 4.9 Hz, 1H, H-3), 7.21 (d, J = 8.4 Hz, 1H, H-6), 6.67 (d, J = 8.4 Hz, 1H, H-7), 6.15 – 6.07 (m, 2H, H-d, d'), 5.89 – 5.77 (m, 2H, H-c, c'), 2.57–2.51 (m, 1H, H-f), 2.35 (t, J = 7.3 Hz, 2H, H-13), 2.20 (s, 3H, H-a), 1.96 (t, J = 7.2 Hz, 2H, H-18), 1.67–1.57 (m, 2H, H-14), 1.57–1.46 (m, 2H, H-17), 1.42–1.24 (m, 4H, H-15/16), 1.04 (dd, J = 6.6, 2.8 Hz, 6H, H-g). ^{13}C NMR (101 MHz, DMSO-d_6) δ (ppm) 172.16 (C-12), 169.14 (C-19), 168.60 (C-8), 149.70 (C-2), 144.38 (C-9), 133.84 (C-4), 126.77 (C-6), 125.53 (C-10), 122.39 (C-3), 118.24 (C-5), 111.49 (C-7), 90.07 (C-e), 89.85 (C-b), 73.48 (C-d/d'), 72.58 (C- d/d'), 70.60 (C-c'), 69.75 (C-c), 35.55 (C-13), 32.27 (C-18), 30.82 (C-f), 28.51 (C-15), 28.41 (C-16), 25.31 (C-14), 25.08 (C-17), 22.25 (C-g, g'), 18.20 (C-a).

Chlorido(N^{20}-hydroxy-N^{11}-(8-hydroxyquinolin-5-yl)octanediamide-κ^2N,O)(η^5-pentamethylcyclopentadienyl)rhodium(III) ***1c***

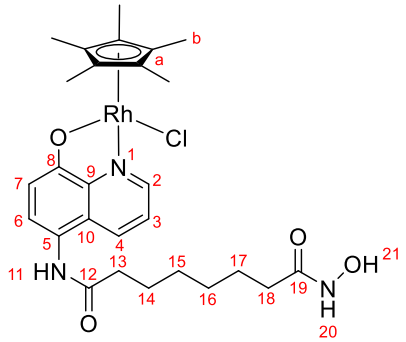

1c

The synthesis was performed according to the general procedure using **L1** (166 mg, 0.50 mmol), $NaHCO_3$ (46 mg, 0.55 mmol), and $[Rh(Cp^*)Cl_2]_2$ (156 mg, 0.25 mmol) to afford **1c** as an orange solid (287 mg, 95%). HRMS (ESI^+): *m/z* 568.1671 $[M - Cl]^+$ (m_{calc} = 568.1677). EA calculated for

$C_{27}H_{35}ClN_3O_4Rh \cdot 1.5H_2O$: C 51.40, H 6.07, N 6.66%; found: C 51.40, H 6.29, N 6.80%. ^{1}H NMR (400 MHz, DMSO-d_6) δ (ppm) 10.34 (s, 1H, H-20), 9.45 (s, 1H, H-11), 8.75 (d, J = 4.4 Hz, 1H, H-2), 8.65 (s, 1H, H-21), 8.07 (d, J = 8.3 Hz, 1H, H-4), 7.55 (dd, J = 8.3, 4.9 Hz, 1H, H-3), 7.13 (d, J = 8.2 Hz, 1H, H-6), 6.62 (d, J = 8.3 Hz, 1H, H-7), 2.34 (t, J = 7.3 Hz, 2H, H-13), 1.95 (t, J = 7.3 Hz, 2H, H-18), 1.69–1.57 (m, 17H, H-b/14), 1.56–1.46 (m, 2H, H-17), 1.40–1.26 (m, 4H, H-15/16). ^{13}C{^{1}H}DEPT-Q (101 MHz, DMSO-d_6) δ (ppm) 172.22 (C-12), 169.13 (C-19), 166.45 (C-8), 147.31 (C-2), 144.53 (C-9), 133.64 (C-4), 127.46 (C-6), 126.23 (C-10), 122.38 (C-3), 116.76 (C-5), 111.69 (C-7), 93.00 (C-a), 92.92 (C-a), 35.53 (C-13), 32.27 (C-18), 28.52 (C-15), 28.41 (C-16), 25.34 (C-14), 25.09 (C-17), 8.47 (C-b).

Chlorido(N^{20}-hydroxy-N^{11}-(ethyl 8-((8-hydroxyquinolin-5-yl)amino)-8-oxooctanoate-κ^2N,O)(η^6-p-cymene)ruthenium(II) ***2a***

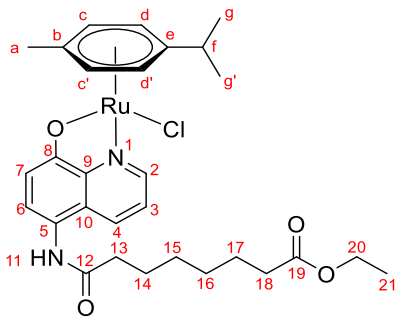

2a

The synthesis was performed according to the general procedure using **L2** (172 mg, 0.50 mmol), $NaHCO_3$ (46 mg, 0.55 mmol), and $[Ru(cym)Cl_2]_2$ (153 mg, 0.25 mmol) to afford **2a** as a dark red solid (250 mg, 81%). HRMS (ESI$^+$): *m/z* 579.1793 $[M - Cl]^+$ (m_{calc} = 579.1791). EA calculated for $C_{29}H_{37}ClN_2O_4Ru \cdot 1.2H_2O$: C 54.79, H 6.25, N 4.41%; found: C 54.45, H 6.20, N 4.81%. ^{1}H NMR (400 MHz, DMSO-d_6) δ (ppm) 9.48 (s, 1H, H-11), 9.19 (d, *J* = 4.4 Hz, 1H, H-2), 8.06 (d, *J* = 8.4 Hz, 1H, H-4), 7.51 (dd, *J* = 8.5, 4.8 Hz, 1H, H-3), 7.12 (d, *J* = 8.4 Hz, 1H, H-6), 6.63 (d, *J* = 8.3 Hz, 1H, H-7), 5.82 – 5.76 (m, 2H, H-d,d'), 5.56 (d, *J* = 5.8 Hz, 1H, H-c'), 5.53 (d, *J* = 5.8 Hz, 1H, H-c), 4.04 (q, *J* = 7.1 Hz, 2H, H-20), 2.72 – 2.60 (m, 1H, H-f), 2.33 (t, *J* = 7.3 Hz, 2H, H-13), 2.28 (t, *J* = 7.3 Hz, 2H, H-18), 2.13 (s, 3H, H-a), 1.64 – 1.58 (m, 2H, H-14), 1.58 – 1.50 (m, 2H, H-17), 1.37 – 1.28 (m, 4H, H-15, 16), 1.17 (t, *J* = 7.1 Hz, 3H, H-21), 1.06 (d, *J* = 6.8 Hz, 6H, H-g, g'). ^{13}C{^{1}H}DEPT-Q (101 MHz, DMSO-d_6) δ (ppm) 173.09 (C-19), 172.34 (C-12), 167.18 (C-8), 149.95 (C-2), 143.58 (C-9), 133.52 (C-4), 126.94 (C-6), 125.61 (C-10), 122.17 (C-3), 117.25 (C-5), 111.62 (C-7), 100.11 (C-e), 98.16 (C-b), 82.56 (C-d'), 81.86 (C-d), 80.56 (C-c'), 80.20 (C-c), 59.81 (C-20), 35.60 (C-13), 33.59 (C-18), 30.50 (C-f), 28.48 (C-15/16), 28.30 (C-15/16), 25.31 (C-14), 24.47 (C-17), 22.05 (C-g/g'), 21.86 (C-g/g'), 18.21 (C-a), 14.24 (C-21).

Chlorido(N^{20}-hydroxy-N^{11}-(ethyl 8-((8-hydroxyquinolin-5-yl)amino)-8-oxooctanoate-κ^2N,O)(η^6-p-cymene)osmium(II) ***2b***

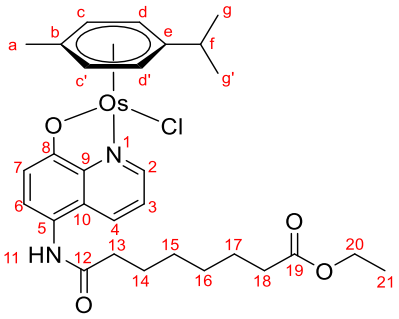

2b

The synthesis was performed according to the general procedure using **L2** (172 mg, 0.50 mmol), $NaHCO_3$ (46 mg, 0.55 mmol), and $[Os(cym)Cl_2]_2$ (201 mg, 0.25 mmol) to afford **2b** as an orange solid (281 mg, 80%). HRMS (ESI^+): *m/z* 669.2358 $[M - Cl]^+$ (m_{calc} = 669.2363). EA calculated for $C_{29}H_{37}ClN_2O_4Os \cdot 1.6H_2O$: C 47.58, H 5.53, N 3.83%; found: C 47.32, H 5.23, N 3.70%. ^1H NMR (400 MHz, DMSO-d_6) δ (ppm) 9.53 (s, 1H, H-11), 9.09 (d, *J* = 4.8 Hz, 1H, H-2), 8.06 (d, *J* = 8.5 Hz, 1H, H-4), 7.49 (dd, *J* = 8.6, 5.0 Hz, 1H, H-3), 7.21 (d, *J* = 8.4 Hz, 1H, H-6), 6.67 (d, *J* = 8.4 Hz, 1H, H-7), 6.14 – 6.08 (m, 2H, H-d,d'), 5.85 (d, *J* = 5.9 Hz, 1H, H-c'), 5.83 (d, *J* = 5.8 Hz, 1H, H-c), 4.05 (q, *J* = 7.1 Hz, 2H, H-20), 2.56 – 2.51 (m, 1H, H-f), 2.35 (t, *J* = 7.4 Hz, 2H, H-13), 2.29 (t, *J* = 7.4 Hz, 2H, H-18), 2.20 (s, 3H, H-a), 1.67 – 1.58 (m, 2H, H-14), 1.58 – 1.51 (m, 2H, H-17), 1.39 – 1.29 (m, 4H, H-15, 16), 1.17 (t, *J* = 7.1 Hz, 3H, H-21), 1.05 (d, *J* = 3.1 Hz, 3H, H-g/g'), 1.03 (d, *J* = 3.1 Hz, 3H, H-g/g'). $^{13}C\{^1H\}$DEPT-Q (101 MHz, DMSO-d_6) δ (ppm) 172.85 (C-19), 172.06 (C-12), 168.58 (C-8), 149.66 (C-2), 144.36 (C-9), 133.80 (C-4), 126.71 (C-6), 125.48 (C-10), 122.32 (C-3), 118.19 (C-5), 111.44 (C-7), 90.03 (C-e), 89.78 (C-b), 73.43 (C-d'), 72.55 (C-d), 70.58 (C-c'), 69.73 (C-c), 59.62 (C-20), 35.48 (C-13), 33.46 (C-18), 30.79 (C-f), 28.38 (C-15/16), 28.20 (C-15/16), 25.18 (C-14), 24.35 (C-17), 22.22 (C-g, g'), 18.16 (C-a), 14.12 (C-21).

Chlorido(N^{20}-hydroxy-N^{11}-(ethyl 8-((8-hydroxyquinolin-5-yl)amino)-8-oxooctanoate-κ^2N,O)(η^5-pentamethylcyclopentadienyl)rhodium(III) ***2c***

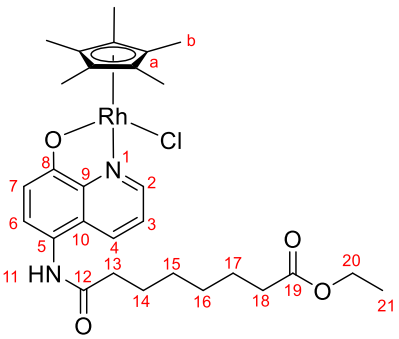

2c

The synthesis was performed according to the general procedure using **L2** (172 mg, 0.50 mmol),

$NaHCO_3$ (46 mg, 0.55 mmol), and $[Rh(Cp^*)Cl_2]_2$ (156 mg, 0.25 mmol) to afford **2c** as a red solid (146 mg, 48%). HRMS (ESI^+): *m/z* 581.1877 $[M - Cl]^+$ (m_{calc} = 581.1881). EA calculated for $C_{29}H_{38}ClN_2O_4Rh \cdot 1.8H_2O \cdot 0.2CHCl_3$: C 52.09, H 6.26, N 4.16%; found: C 51.94, H 6.04, N 4.35%. ^1H NMR (400 MHz, DMSO-d_6) δ (ppm) 9.46 (s, 1H, H-11), 8.75 (d, *J* = 4.4 Hz, 1H, H-2), 8.08 (d, *J* = 8.4 Hz, 1H, H-4), 7.55 (dd, *J* = 8.4, 4.8 Hz, 1H, H-3), 7.14 (d, *J* = 8.4 Hz, 1H, H-6), 6.62 (d, *J* = 8.4 Hz, 1H, H-7), 4.06 (q, *J* = 7.1 Hz, 2H, H-20), 2.35 (t, *J* = 7.3 Hz, 2H, H-13), 2.30 (t, *J* = 7.3 Hz, 2H, H-18), 1.69 – 1.60 (m, 17H, H-14, b), 1.59 – 1.52 (m, 2H, H-17), 1.41 – 1.29 (m, 4H, H-15, 16), 1.18 (t, *J* = 7.1 Hz, 3H, H-21). $^{13}C\{^1H\}$DEPT-Q (101 MHz, DMSO-d_6) δ (ppm) 172.87 (C-19), 172.15 (C-12), 166.45 (C-8), 147.28 (C-2), 144.52 (C-9), 133.61 (C-4), 127.42 (C-6), 126.20 (C-10), 122.33 (C-3), 116.73 (C-5), 111.65 (C-7), 92.96 (C-a), 92.88 (C-a), 59.63 (C-20), 35.47 (C-13), 33.47 (C-18), 28.41 (C-15/16), 28.21 (C-15/16), 25.23 (C-14), 24.37 (C-17), 14.13 (C-21), 8.44 (C-b).

Chlorido(N^{20}-hydroxy-N^{11}-(ethyl 8-((8-hydroxyquinolin-5-yl)amino)-8-oxooctanoate-κ^2N,O)(η^5-pentamethylcyclopentadienyl)rhodium(III) ***2d***

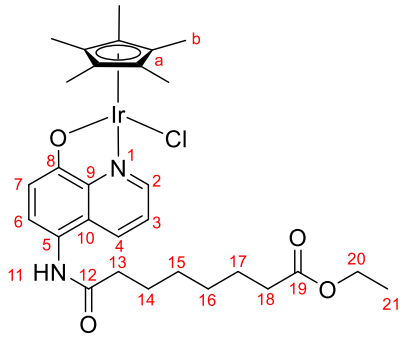

2d

The synthesis was performed according to the general procedure using **L2** (172 mg, 0.50 mmol), $NaHCO_3$ (46 mg, 0.55 mmol), and $[Ir(Cp^*)Cl_2]_2$ (198 mg, 0.25 mmol) to afford **2d** as a yellow solid (254 mg, 72%). HRMS (ESI^+): *m/z* 671.2452 $[M - Cl]^+$ (m_{calc} = 671.2455). EA calculated for $C_{29}H_{38}ClIrN_2O_4 \cdot 1.8C_4H_8O_2 \cdot 0.4C_2H_3N$: C 50.43, H 6.13, N 3.81%; found: C 50.63, H 5.91, N 3.92%. ^1H NMR (300 MHz, DMSO-d_6) δ (ppm) 9.65 (s, 1H, H-11), 8.75 (d, *J* = 4.0 Hz, 1H, H-2), 8.08 (d, *J* = 8.0 Hz, 1H, H-4), 7.53 (dd, *J* = 8.1, 4.8 Hz, 1H, H-3), 7.20 (d, *J* = 8.1 Hz, 1H, H-6), 6.63 (d, *J* = 8.0 Hz, 1H, H-7), 4.05 (d, *J* = 6.9 Hz, 2H, H-20), 2.42 – 2.33 (m, 2H, H-13), 2.29 (t, *J* = 7.1 Hz, 2H, H-18), 1.75 – 1.58 (m, 17H, H-14, b), 1.58 – 1.51 (m, 2H, H-17), 1.44 – 1.25 (m, 4H, H-15, 16), 1.17 (t, *J* = 6.9 Hz, 3H, H-21). $^{13}C\{^1H\}$DEPT-Q (101 MHz, DMSO-d_6) δ (ppm) 172.91 (C-19), 172.31 (C-12), 167.49 (C-8), 147.45 (C-2), 145.06 (C-9), 133.97 (C-4), 127.27 (C-6), 126.37 (C-10), 122.54 (C-3), 118.16 (C-5), 112.03 (C-7), 84.52 (C-a), 59.65 (C-20), 35.45 (C-13), 33.49 (C-18), 28.41 (C-15/16), 28.22 (C-15/16), 25.24 (C-14), 24.38 (C-17), 14.15 (C-21), 8.46 (C-b).

Stability in aqueous solution and Cl/H_2O ligand exchange

The hydrolytic stability of complexes **1a–1c** was studied by dissolving 2-3 mg/mL in 20% MeOD-d_4/D_2O, and ^{1}H NMR spectra were recorded after 0, 0.5, and 4 h (Figures S1–S3). The formation of aqua complexes was confirmed by the addition of 1 eq. of $AgNO_3$. Suppression of aqua/chlorido ligand exchange reactions was investigated by dissolving the complexes in solutions containing 104 mM NaCl in 20% MeOD-d_4/D_2O.

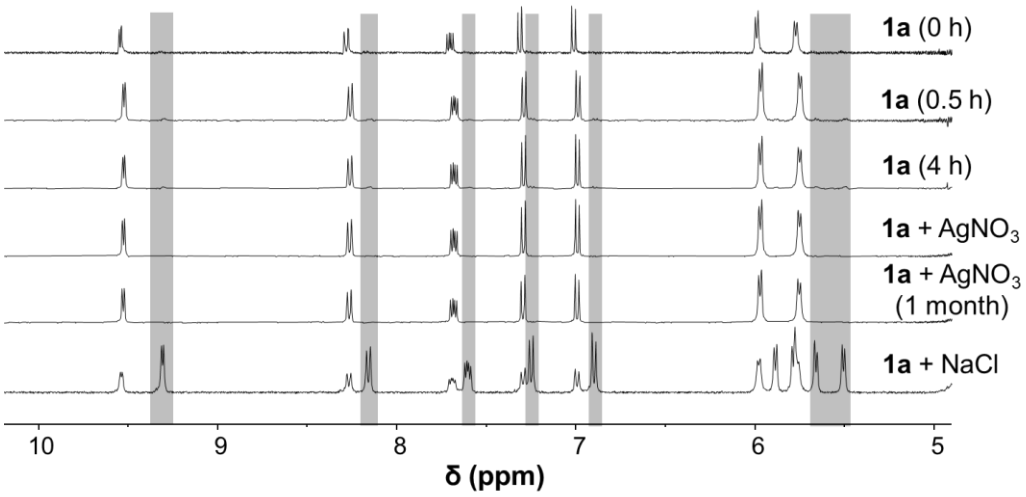

Figure S1. ^{1}H NMR spectra of **1a** in 20% MeOD-d_4/D_2O recorded 0, 0.5, and 4 h after dissolution, after addition of 1 eq. $AgNO_3$, and in the presence of NaCl (104 mM).

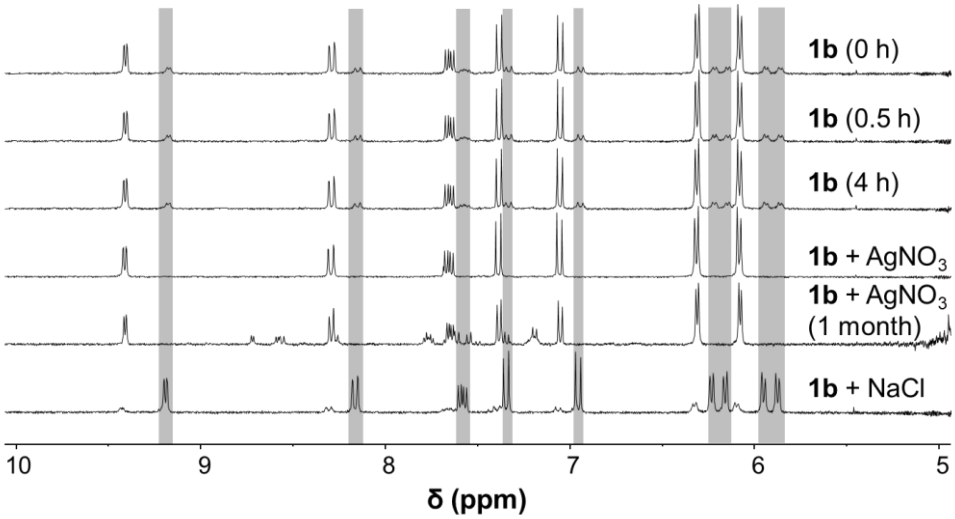

Figure S2. ^{1}H NMR spectra of **1b** in 20% MeOD-d_4/D_2O recorded 0, 0.5, and 4 h after dissolution, after addition of 1 eq. $AgNO_3$, and in the presence of NaCl (104 mM).

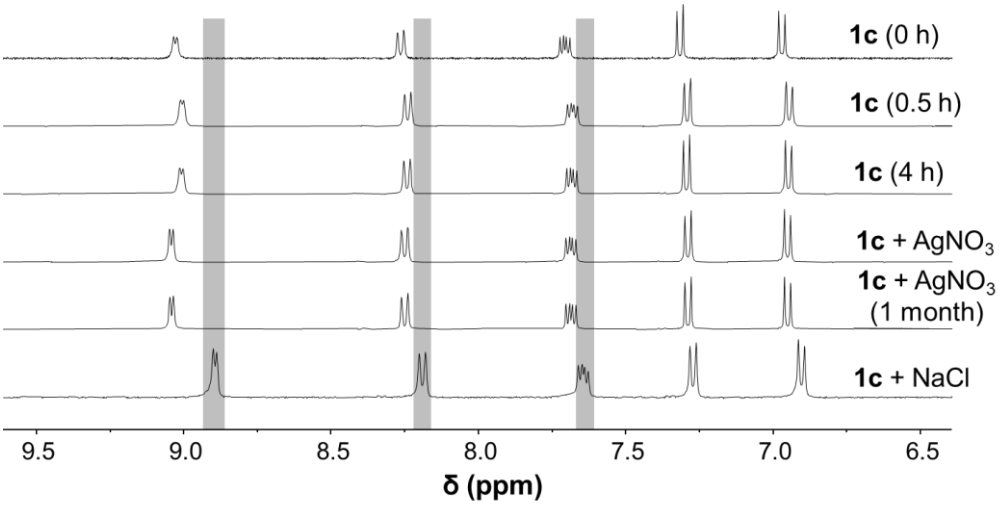

Figure S3. ^{1}H NMR spectra of **1c** in 20% MeOD-d_4/D_2O recorded 0, 0.5, and 4 h after dissolution, after addition of 1 eq. $AgNO_3$, and in the presence of NaCl (104 mM).

Sulforhodamine B antiproliferative activity assay

HCT116 and NCI-H460 cells were supplied by ATCC, while A2780 and A2780cis cells were supplied by ECACC. The cells were grown in α-MEM (Life Technologies) supplemented with 5% foetal calf serum (Moregate Biotech) at 37 °C in a humidified incubator with 5% CO_2. The cells were seeded at 750 (HCT116, NCI-H460) or 1000 (A2780, A2780cis) cells/well in 96-well plates and left to settle for 24 h.

For the single-dose study, each compound was added to the wells at a final concentration of 20 μM, containing 0.5% DMSO. To determine the IC_{50} values, the compounds were added in a series of 3-fold dilutions, containing a maximum of 0.5% DMSO at the highest concentration. Both assays were terminated after 72 h by addition of 10% trichloroacetic acid (Merck Millipore) at 4 °C for 1 h. The cells were stained with 0.4% sulforhodamine B (Sigma-Aldrich) in 1% acetic acid for 30 min in the dark at room temperature and then washed with 1% acetic acid to remove unbound dye. The stain was dissolved in unbuffered Tris base (10 mM; Serva) for 30 min on a plate shaker in the dark and quantified on a BioTek EL808 microplate reader at an absorbance wavelength of 490 nm with 450 nm as the reference wavelength to determine the percentage of cell growth inhibition by determining the absorbance of each sample relative to negative (DMSO) and no-growth controls (day 0). The cell viability ratios were calculated with Microsoft Excel® for Microsoft 365, and the presented cell viability values for single dose studies were the mean of at least two independent experiments where the analysis for each compound was repeated five times. The IC_{50} values were calculated with SigmaPlot 14.0 using a three-parameter logistic sigmoidal dose–response curve between the calculated growth inhibition and the compound concentration. The presented IC_{50} values are the means of at least 3 independent experiments, where 10 concentrations were tested in duplicate for each compound.

Table S1. Single concentration (20 μM) antiproliferation SRB assay for the synthesised compounds and cisplatin in A2780 and A2780cis cells (72 h). [a] No viable A2780 cells were detected.

Compound	Cell Viability (%)	
	A2780	A2780cis
L1	_ [a]	0.2 ± 1.6
1a	41 ± 7	44 ± 15
1b	55 ± 8	63 ± 11
1c	2.4 ± 0.4	4.1 ± 2.5
L2	4.5 ± 1	13 ± 6
2a	61 ± 5	79 ± 17
2b	52 ± 5	70 ± 11
2c	6.6 ± 2.5	17 ± 10
2d	14 ± 3	31 ± 11
Cisplatin	2.3 ± 1.3	40 ± 7

HDAC inhibitory activity

HDAC1 and HDAC6 inhibitory activity assays were performed as described previously.[7] Briefly, reactions were carried out in buffer containing 50 mM HEPES, 140 mM NaCl, 10 mM KCl, pH 7.4, supplemented with 1 mg/mL bovine serum albumin (BSA) and 1 mM tris(2-carboxyethyl)phosphine (TCEP). Recombinant HDAC proteins were preincubated with a dilution series of the tested inhibitors in 384-well plates (30 μL total volume; Corning, NY, USA) at 37 °C for 15 min. Subsequently, 10 μL of Ac-GAK-Ac-AMC substrate (final concentration 10 μM; Bachem, Bubendorf, Switzerland) was added, and the reactions proceeded for an additional 30 min. Reactions were terminated by adding 25 μL of trypsin solution (4 mg/mL stock), and the released aminomethylcoumarin was quantified using a CLARIOstar plate reader (BMG Labtech GmbH, Ortenberg, Germany) at $\lambda_{ex}/\lambda_{em}$ = 365/440 nm. HDAC inhibition was calculated using corresponding non-inhibited reactions as controls. Inhibition data were fitted in GraphPad Prism (GraphPad Software, San Diego, CA, USA) using nonlinear regression analysis.

HDAC inhibitory activity in cells

Tubulin acetylation levels were used as a surrogate marker to determine the inhibitory potency of the test compounds in cells using a protocol described previously.[8] Following the reported procedure,[7] RPMI-8226 lymphoblasts (106 cells/mL) in an RPMI-1640 medium supplemented with 10% FBS were incubated in 96-well plates (90 μL). A dilution series of 10 μL of stock inhibitor solutions in PBS (10 μL) was added to the cells and incubated at 37 °C for 6 h. The plate was centrifuged at 500×g at 22 °C for

5 min, the supernatant discarded, and cells resuspended in 80 µL of lysis buffer (20 mM Tris, 4 M urea, 5 mM $MgCl_2$, 0.5% Triton X-100, pH 8.2) supplemented with protease inhibitors (cOmplete EDTA-free protease inhibitors cocktail, Roche, Basel, Switzerland) and benzonase (2U/mL, Merck, Darmstadt, Germany). Following a 5-min incubation at 22 °C, a 4× SDS-PAGE sample buffer was added and the sample was heated to 95 °C for 5 min. Samples (104 cells/lane) were separated by SDS-PAGE and levels of acetylated tubulin (Ac-tub) were determined by quantitative Western blotting.

Western blotting analysis

The Western blotting analysis procedure was adapted as described previously.[7] Samples separated by SDS-PAGE were transferred onto a PVDF membrane using a Trans-Blot Turbo RTA Mini PVDF Transfer kit (Bio-Rad, Hercules, CA, USA). The membrane was blocked with 5% BSA in TBS (50 mM Tris-HCl, 150 mM NaCl, pH 7.4) and incubated with the primary antibody mix in 5% BSA in TBS at 4 °C overnight. The antibodies used were anti-alpha tubulin (1:4000 dilution, rabbit, #Ab18251, Abcam, Cambridge, UK), antiacetylated tubulin (1:2500 dilution, mouse, #T7451, Sigma-Aldrich, St. Louis, MO, USA), and anti-acetylated histone H3 (Lys9/Lys14) (1:2000 dilution, rabbit, #9677, Cell Signaling, Danvers, MA, USA). On the next day, the membrane was washed in TBS + 0.2% Tween 20, and further incubated in a mix of secondary antibodies comprising Alexa Fluor 568-donkey anti-rabbit IgG (0.4 µg/mL, #A10042, Invitrogen, Waltham, MA, USA) and Alexa Fluor 488goat anti-mouse IgG (0.4 µg/mL, #A11029, Invitrogen, Waltham, MA, USA) at 22 °C for 1 h. Bands were visualised using a Typhoon FLA9500 fluorescence imager (GE Healthcare BioSciences, Little Chalfont, UK) and signal intensities were quantified using Quantity One 1-D Analysis Software (Bio-Rad, Hercules, CA, USA). Signals of Ac-tubulin were normalised to the total tubulin load and the absolute amount of acetylation was determined relative to purified α-tubulin standards with known acetylation levels.

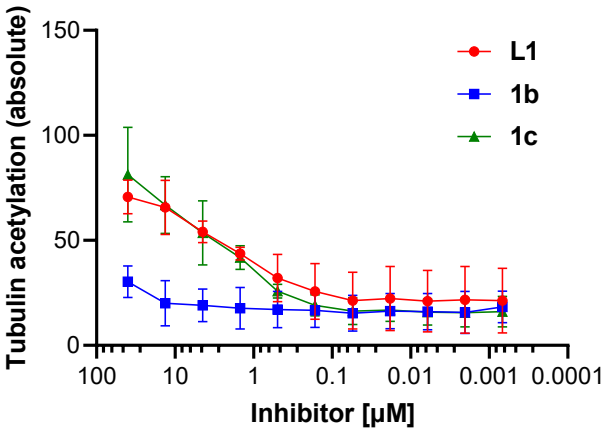

Figure S4. Quantification of the tubulin acetylation status after treatment with **L1**, **1b**, and **1c**.

Cellular accumulation studies

Adapting a literature method, all studies were carried out using HCT116 human colorectal carcinoma cells, supplied by ATCC.[9] The cells were grown in α-MEM (Life Technologies), supplemented with 5% foetal calf serum (Moregate Biotech) at 37 °C in a humidified incubator with 5% CO_2. Cell uptake studies were performed in 24-well plates using 100,000 cells per well in 750 µL of medium. Cells were allowed to settle for 24 h before starting each experiment. In general, each concentration and time point was investigated in triplicate in each individual plate, and each condition was repeated in three independent experiments. Each plate included adsorption correction wells to account for plastic adsorption. The final volume in each well after addition of complexes was 1 mL in all experiments. At the end of each experiment, the medium was removed, and each well was washed twice with 0.5 mL cold PBS. The plates were stored in a freezer until ICP-MS analysis.

For ICP-MS analysis, the cells were digested in the 24-well plates. HNO_3 (200 µL, 69%) was added to each well and the samples were allowed to digest for 2 h. The samples were diluted by transferring 150 µL of the digest to a 15 mL falcon tube and adding MQ-H_2O to obtain a final volume of 3 mL. Pt was added as the internal standard at a final concentration of 3 µg/L. The solutions were quantitatively analysed for the desired elements on an Agilent 8900 ICP-QQQ-MS in He mode to reduce potential polyatomic interferences. The samples were introduced using an Agilent SPS4 autosampler and a MicroMist nebuliser. The carrier gas flow rate was 1.05 L/min, plasma gas flow rate was 15.0 L/min, RF power 1600 W, sample depth 9.0 mm. When analysing the cell samples, a blank and a 3 µg/L calibration standard were measured as quality controls after every 20 samples. The monitored masses were ^{99}Ru, ^{101}Ru, ^{103}Rh, ^{188}Os, ^{189}Os, ^{194}Pt and ^{195}Pt. Ru, Rh, Os, and Pt calibration standards (3 µg/L) were prepared from their 1000 µg/mL standard stock solutions, diluting with a matrix-matched solution with regard to HNO_3 concentration. Calibration standards of Ru, Rh, and Os with concentrations of 0.2, 0.5, 1, 3 and 5 µg/L were used. The LOD was defined as 3.3× the standard deviation of the blank samples divided by the slope of the calibration curve. The LOQ was defined as 10× the standard deviation of the blank samples divided by the slope of the calibration curve.

Due to the different mass between Ru, Os, Rh and varying IC_{50} values between complexes, accumulation ratios reflecting the efficiency of cellular uptake for different metals, initial concentrations, and incubation times were calculated respectively for better comparison using:

$$Accumulation\ ratio = \frac{[M_{ICP}]}{[M_{initial}]} \qquad \text{Eq. S1}$$

where

$[M_{ICP}]$ = average metal concentration detected by ICP-MS after correction (µM)

$[M_{initial}]$ = IC_{50} or $2IC_{50}$ (µM)

Table S2. Time and concentration dependence of the intracellular accumulation of **1a**–**1c**, and [Rh(Cp*)(HQ)Cl] **A** (n = 3) in HCT-116 cancer cells.

Compound	Ru, Os or Rh ng/100,000 cells			
	4 h@IC_{50}	4 h@$2IC_{50}$	24 h@IC_{50}	24 h@$2IC_{50}$
1a	1.7 ± 0.5	3.1 ± 0.9	2.5 ± 1.0	5.6 ± 1.5
1b	8.3 ± 5.0	18 ± 13	22 ± 13	45 ± 26
1c	0.065 ± 0.059	0.19 ± 0.01	0.11 ± 0.03	0.20 ± 0.03
A	0.14 ± 0.05	0.097 ± 0.029	0.16 ± 0.07	0.27 ± 0.07

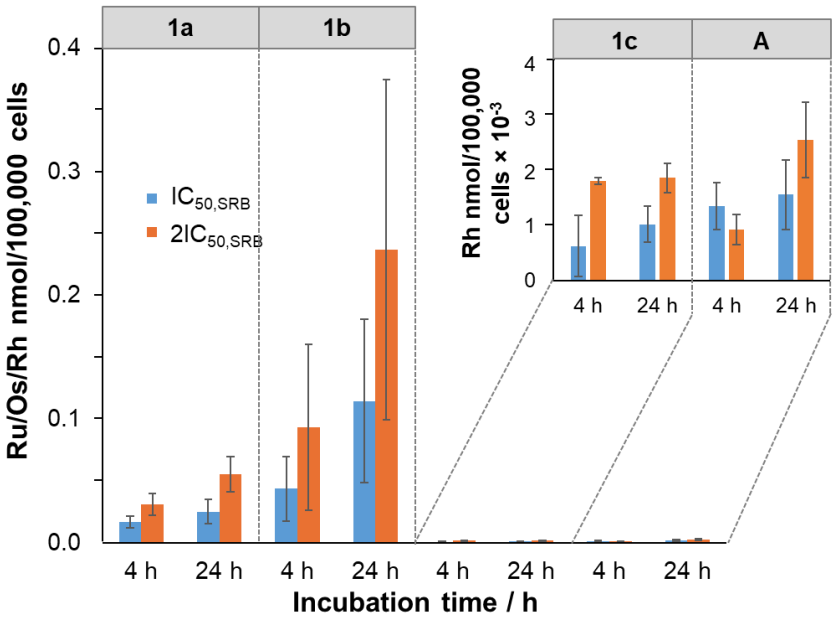

Figure S5. Time and concentration dependence of the intracellular accumulation of **1a**–**1c**, and [Rh(Cp*)(HQ)Cl] **A** in HCT-116 cells (n = 3), error bars represent ± SD.

X-ray diffraction analysis

Table S3. Crystal data and structure refinement for crystal **1c**·½H_2O.

CCDC number	2520772
Empirical formula	$C_{27}H_{35}ClN_3O_4Rh \cdot ½H_2O$
Formula weight	612.95
Temperature/K	120.0(1)
Crystal system	monoclinic
Space group	$P2_1/c$
a/Å	21.6982(3)
b/Å	14.3489(3)
c/Å	8.99650(15)
α/°	90
β/°	98.2961(15)
γ/°	90
Volume/Å^3	2771.70(9)
Z	4
ρ_{calc} g/cm^3	1.469
μ/mm^{-1}	6.188
F(000)	1268.0
Crystal size/mm^3	0.125 × 0.05 × 0.05
Radiation	Cu Kα (λ = 1.54184)
2Θ range for data collection/°	7.41 to 135.472
Index ranges	-26 ≤ h ≤ 23, -16 ≤ k ≤ 17, -10 ≤ l ≤ 10
Reflections collected	22355
Independent reflections	5020 [R_{int} = 0.0619, R_{sigma} = 0.0494]
Data/restraints/parameters	5020/105/389
Goodness-of-fit on F^2	1.057
Final R indexes [I>=2σ (I)]	R_1 = 0.0535, wR_2 = 0.1244
Final R indexes [all data]	R_1 = 0.0672, wR_2 = 0.1323
Largest diff. peak/hole / e Å^{-3}	1.22/-1.91

Table S4. Selected bond lengths (Å) and angles (°) for crystal of **1c**·½H_2O.

Bond	**Bond length (Å)**
Rh1–N1	2.106(4)
Rh1–O1	2.109(4)
Rh1–Cl1	2.399(2)
Rh1–Cp*$_{centroid}$	1.757
C12–N11	1.336(5)
C12–O23	1.237(5)
O22–C19	122(1)
N20–C19	1.34(1)
O21–N20	1.399(9)
Bond	**Bond angle (°)**
N1–Rh1–O1	79.4(2)
O1–Rh1–Cl1	87.65(16)
N1–Rh1–Cl1	82.99(13)
N11–C12–O23	123.2(4)
O22–C19–N20	123.4(9)
C19–N20–O21	122.0(7)

Table S5. Hydrogen-bond interaction in the crystal structure of **1c**·½H_2O.

D-H···A	**D-H** (Å)	**H···A** (Å)	**D···A** (Å)	**D-H···A** (°)
HO–H···Cl1	0.85	2.419	3.23(2)	161
HO–H···O21	0.85	2.104	2.83(3)	143
N11–H···O23	0.88	1.934	2.802(5)	168.9
N20–H···O22	0.88	1.805	2.677(8)	170.6
O21–H···O1	0.84	1.74	2.563(9)	166

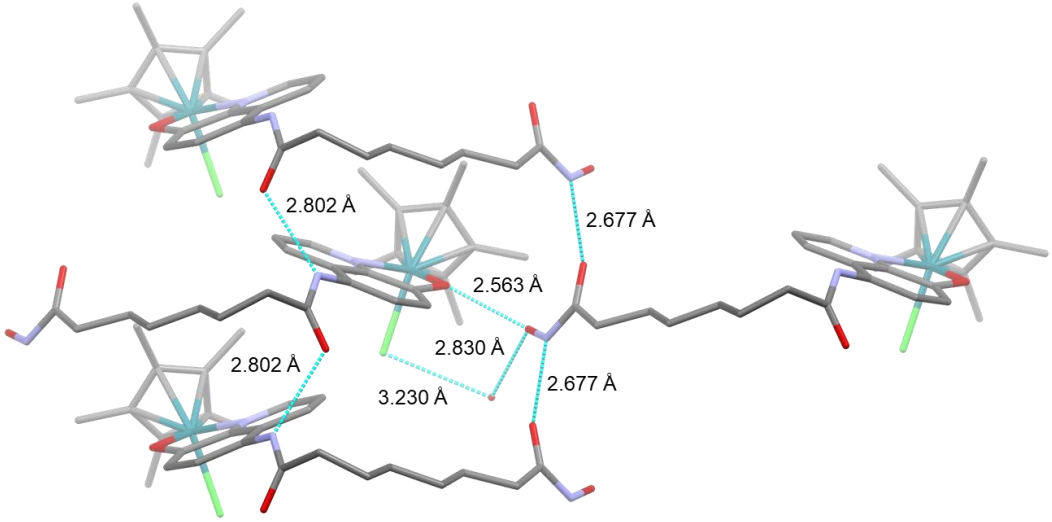

Figure S6. Packing arrangements in the crystal structure of **1c**·½H_2O showing the intermolecular H bonds and the distances between the donor and acceptor atoms.

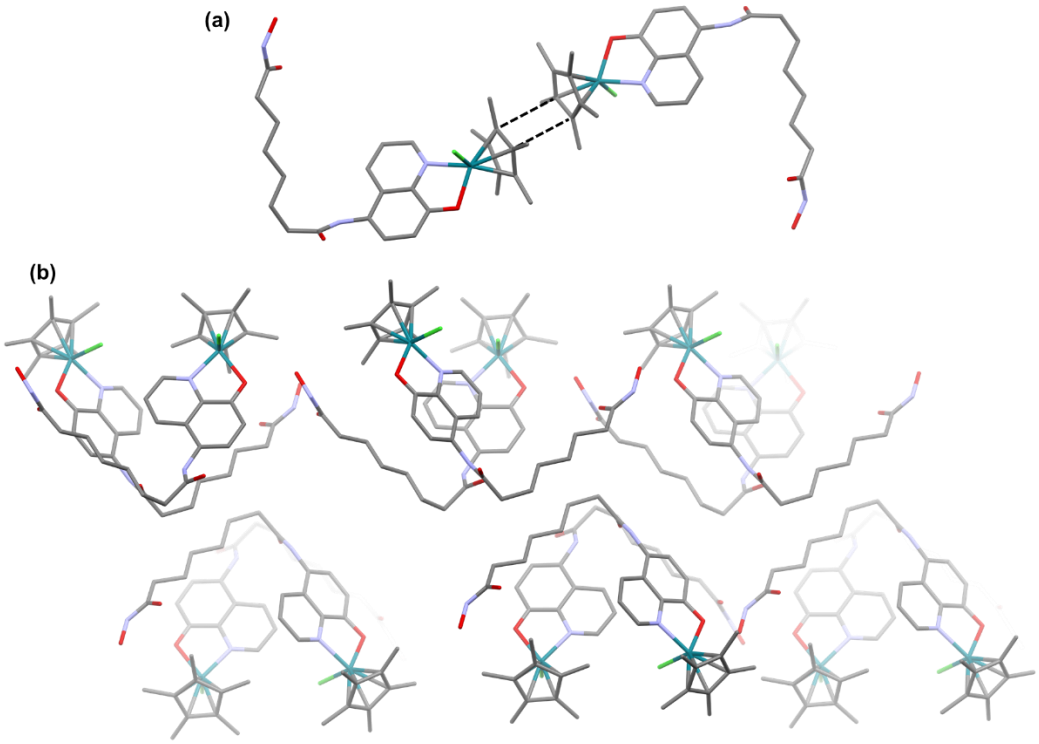

Figure S7. (a) π-stacking between the Cp* rings of neighbouring molecules of **1c** indicated with dashed lines for the closest C atoms (3.652 Å) and (b) packing arrangements in the crystal structure of **1c**·½H_2O.

In silico prediction of ADME

The absorption, distribution, metabolism, and excretion properties of **L1** were calculated with the SwissADME online software (http://www.swissadme.ch).[10] The SMILES notation of **L1** was introduced into the online software to predict the drug-likeness score.

Table S6. ADME parameters for ligand **L1**.

Physiochemical Properties	
Molecular weight (g/mol)	331.37
Heavy atoms	24
Aromatic heavy atoms	10
Fraction Csp^3	0.35
Rotatable bonds	10
H-bond acceptors	5
H-bond donors	4
Molar refractivity	90.65
TPSA ($Å^2$)	111.55
Lipophilicity and water solubility	
Consensus log $P_{o/w}$	1.75
ESOL log S	-2.45
ESOL Solubility (mg/mL)	1.18
ESOL Solubility (mol/L)	3.55e-03
ESOL Class	Soluble
Ali log S	-3.39
Ali Solubility (mg/mL)	1.36e-01
Ali Solubility (mol/L)	4.09e-04
Ali Class	Soluble
Silicos-IT logSw	-4.95
Silicos-IT Solubility (mg/mL)	3.69e-03
Silicos-IT Solubility (mol/L)	1.11e-05
Silicos-IT class	Moderately soluble

Table S6. Cont'd.

Pharmacokinetics	
GI absorption	High
BBB permeant	No
P-gp substrate	Yes
CYP1A2 inhibitor	No
CYP2C19 inhibitor	No
CYP2C9 inhibitor	No
CYP2D6 inhibitor	No
CYP3A4 inhibitor	No
log K_p (cm/s)	-7.3
Drug-likeness	
Lipinski violations	0
Ghose violations	0
Veber violations	0
Egan violations	0
Muegge violations	0
Bioavailability Score	0.55
Medicinal chemistry	
PAINS alerts	0
Brenk alerts	3
Lead-likeness violations	1
Synthetic Accessibility	2.35

Molecular docking

The structures of the docked molecules were built from the molecular structures of **1c** and SAHA[11] (CCDC code: 830152). All geometry optimisation calculations were carried out using Gaussian D.01 version.[12] All optimisations and harmonic frequency calculations were performed at the density functional theory (DFT) level using the Perdew–Burke–Ernzerhof hybrid functional (PBE0)[13] in combination with Ahlrichs full electron def2-TZVP basis set,[14] corrected with Grimme's dispersion correction with Becke-Johnson damping[15] (D3BJ). The solvation model based on density[16] (SMD) was used to model implicit solvation, while acetone was used for the metal complex and water for SAHA. All optimised structures were confirmed to reach the potential energy minima by absence of imaginary frequencies.

The protein structure (PDB ID: 5EEI) was obtained from the Research Collaboratory for Structural Bioinformatics (RCSB) Protein Databank (PDB).[17] The water molecules and other undesirable molecules were removed with PyMOL.[18]

All docking simulations were performed using the GOLD suite.[19] Missing parameters for metals and other modifications were implemented according to Sciortino *et al*.[20] The protein structure was treated as rigid during docking, as the crystallographic structure feature the ideal configuration for binding of the hydroxamic acid group to the Zn(II) ion. Blind molecular docking was performed by defining an evaluation sphere with a radius of 20 Å. Binding modes were predicted using the GoldScore (GS) scoring function. The scaffold match constraint (SMC) was applied, while the heavy atoms of the hydroxamic acid group (O-C-N-O) were used as a complete scaffold.[21] Docking results were analysed and visualised with GOLD and BIOVIA Discovery Studio Visualizer.[22]

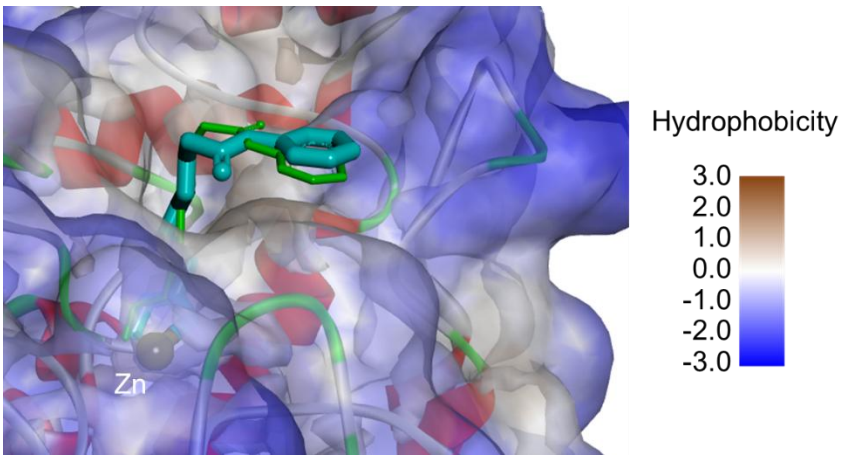

Figure S8. The conformation of SAHA co-crystallised in the catalytic domain 2 of HDAC6 (PDB ID 5eei) and compared to a pose of a docking experiment using GOLD. The protein surface was rendered to indicate hydrophobic areas on the protein.

NMR spectra and ESI-mass spectra

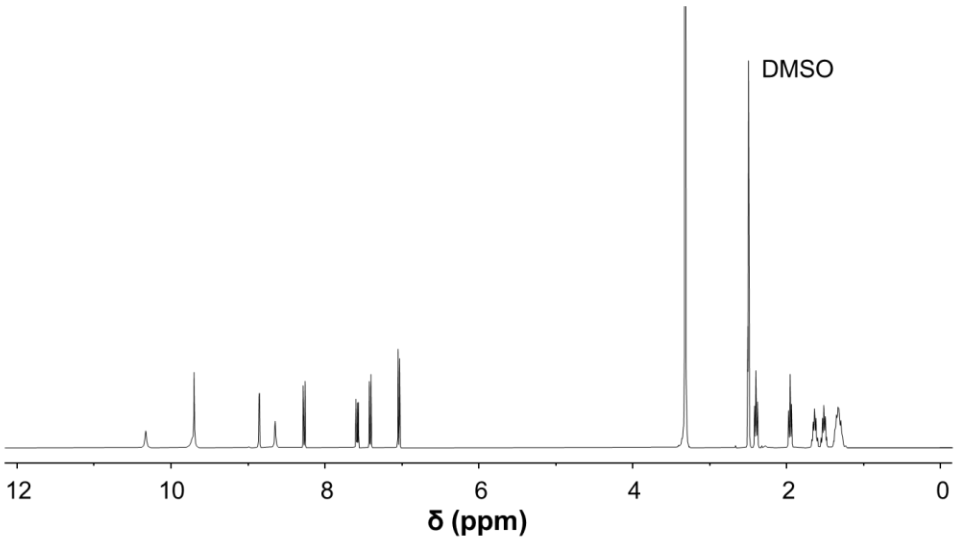

Figure S9. ^{1}H NMR spectrum of **L1** in DMSO-d_6.

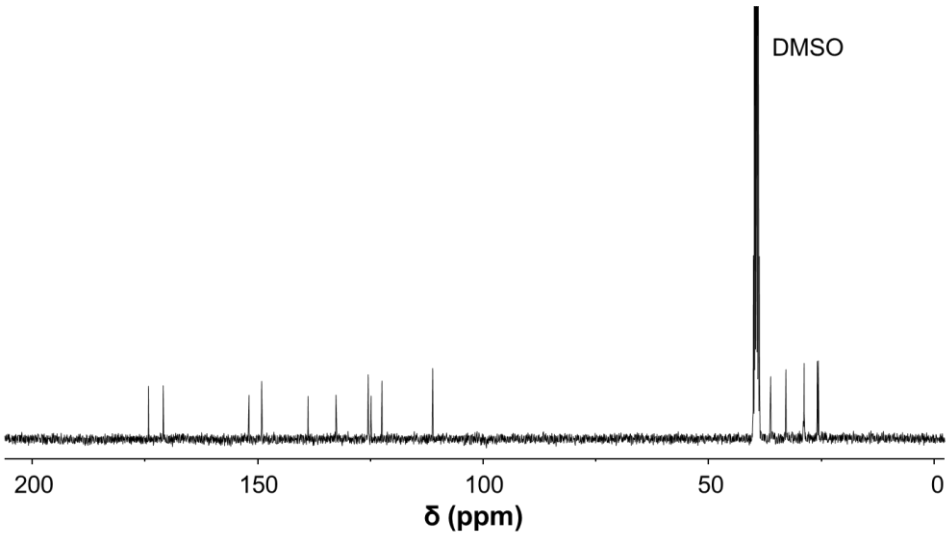

Figure S10. $^{13}C\{^{1}H\}$ NMR spectrum of **L1** in DMSO-d_6.

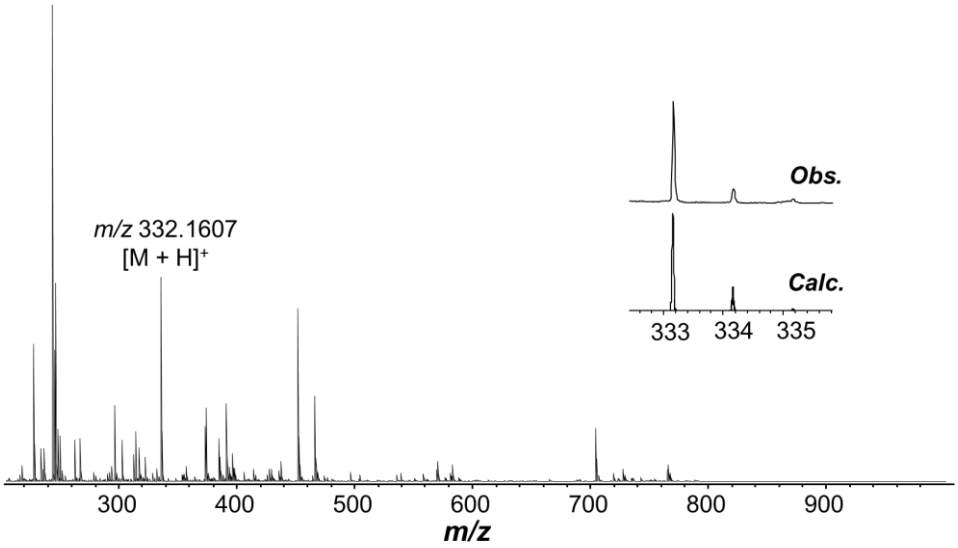

Figure S11. HR-ESI-mass spectrum (MeOH) of **L1**. The inset is the observed isotopic pattern (top) for the $[M + H]^+$ peak compared to the simulated isotopic pattern (bottom).

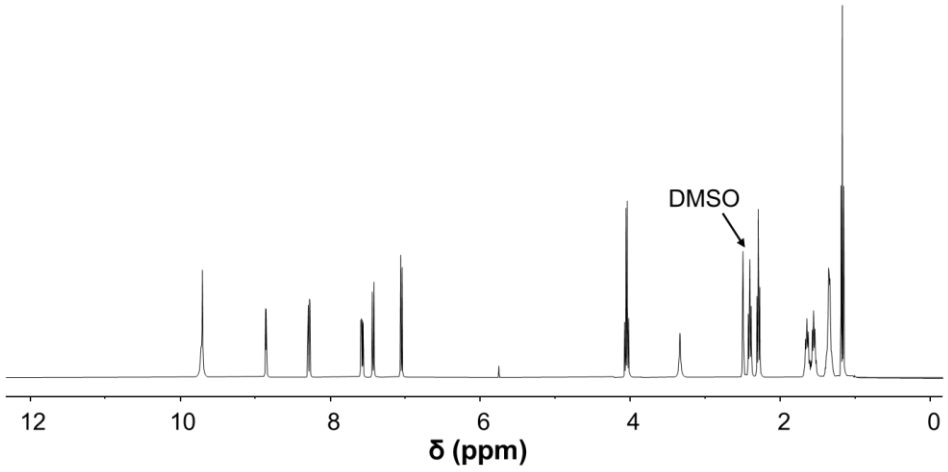

Figure S12. ^{1}H NMR spectrum of **L2** in DMSO-d_6.

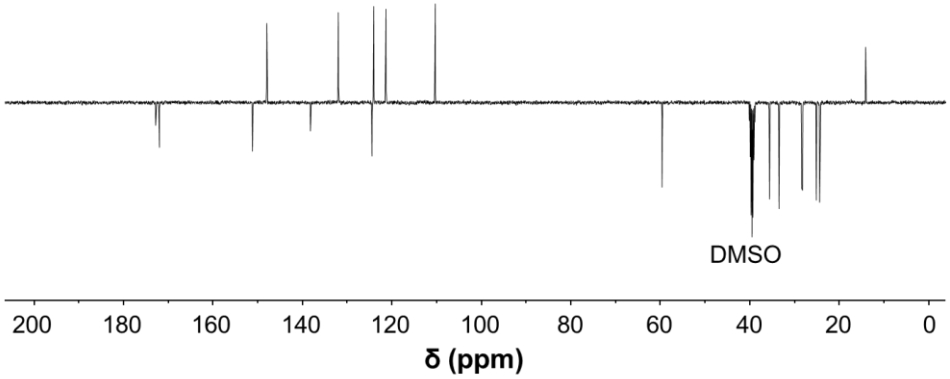

Figure S13. $^{13}C\{^{1}H\}$ DEPT-Q NMR spectrum of **L2** in DMSO-d_6.

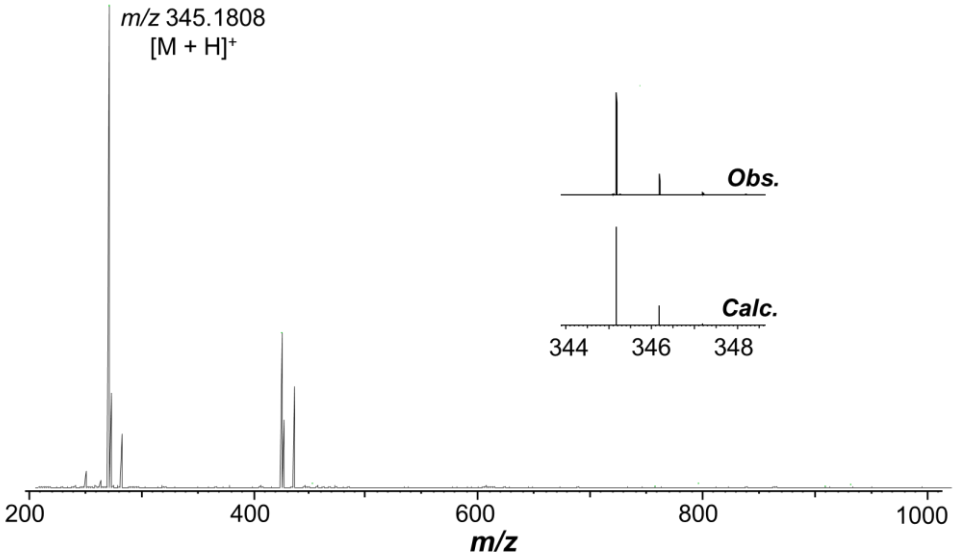

Figure S14. HR-ESI-mass spectrum (MeOH) of **L2**. The inset is the observed isotopic pattern (top) for the $[M + H]^+$ peak compared to the simulated isotopic pattern (bottom).

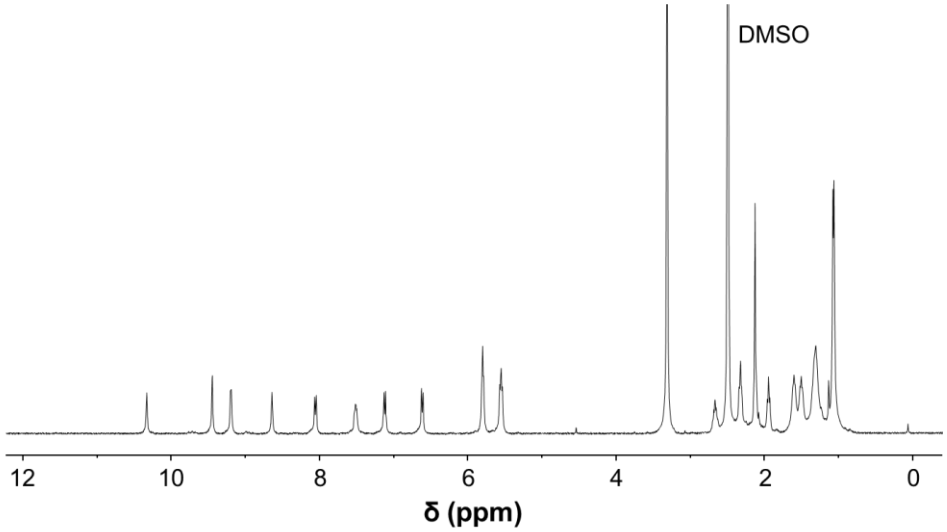

Figure S15. ^{1}H NMR spectrum of **1a** in DMSO-d_6.

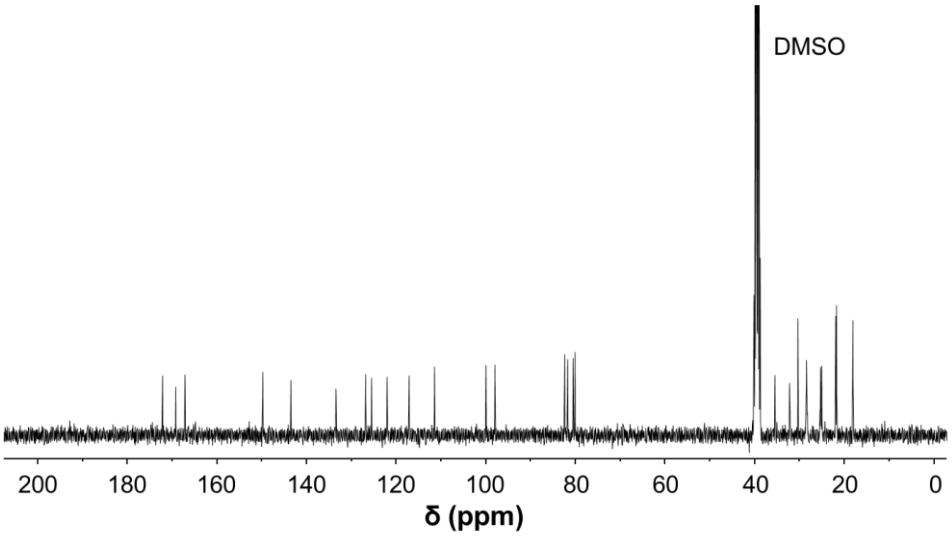

Figure S16. $^{13}C\{^{1}H\}$ NMR spectrum of **1a** in DMSO-d_6.

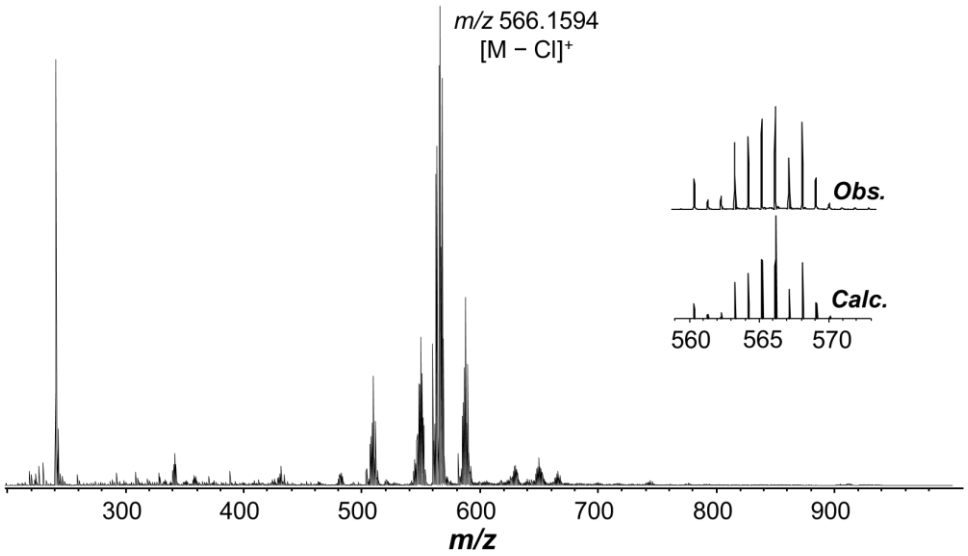

Figure S17. HR-ESI-mass spectrum (MeOH) of **1a**. The inset is the observed isotopic pattern (top) for the $[M - Cl]^+$ peak compared to the simulated isotopic pattern (bottom).

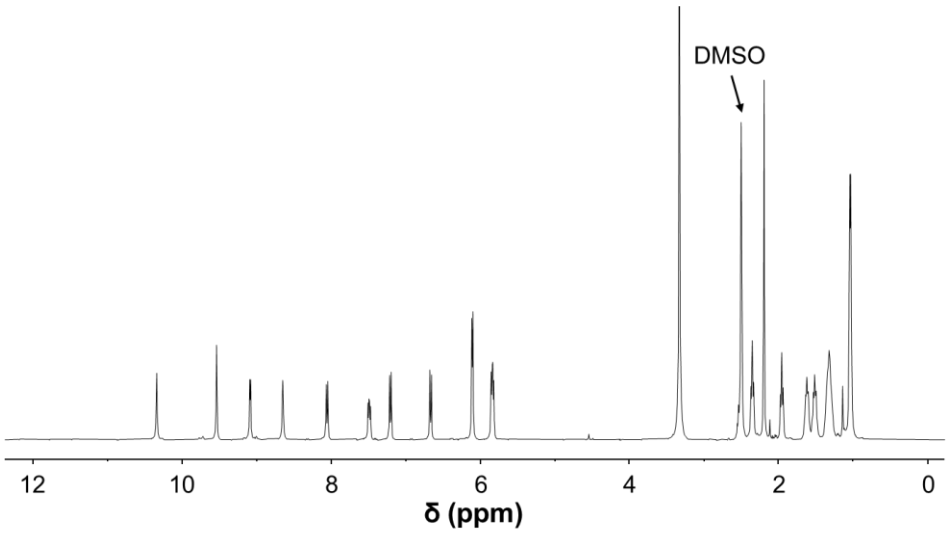

Figure S18. ^{1}H NMR spectrum of **1b** in DMSO-d_6.

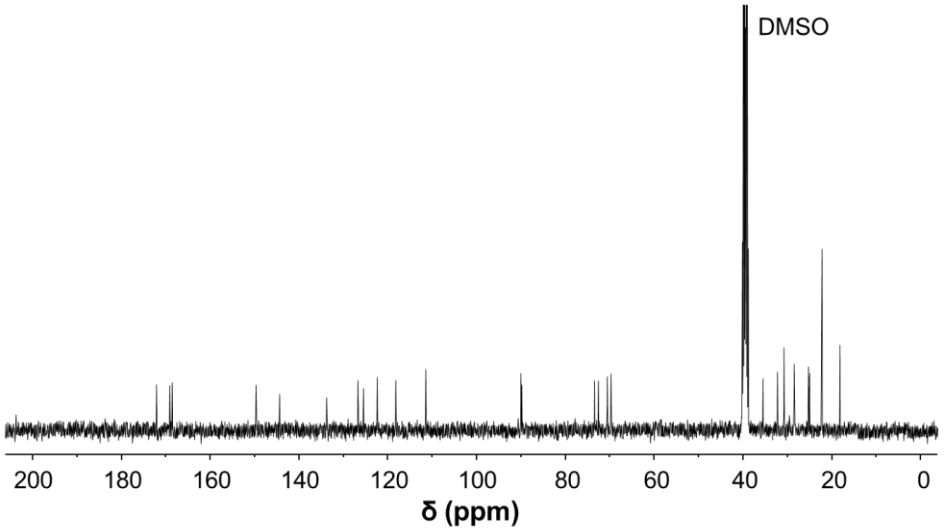

Figure S19. $^{13}C\{^{1}H\}$ NMR spectrum of **1b** in DMSO-d_6.

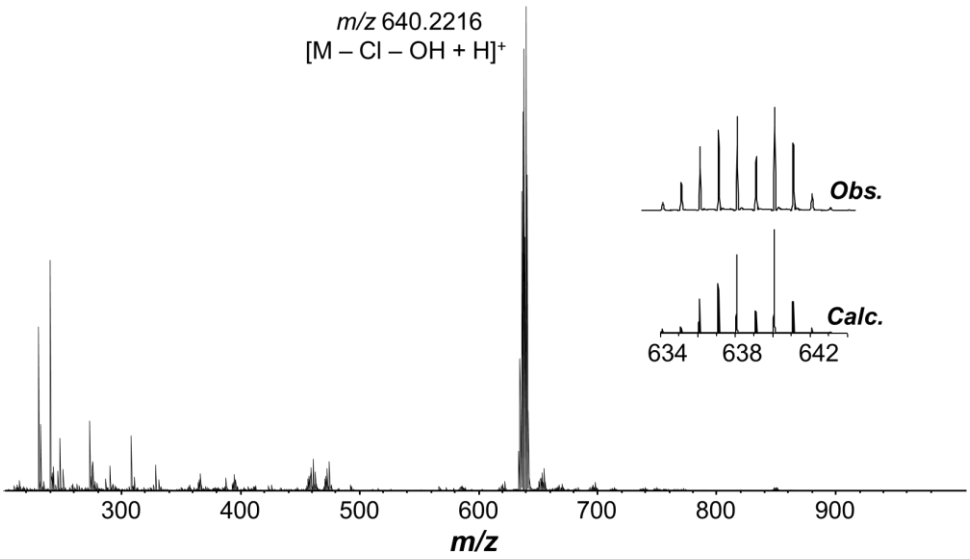

Figure S20. HR-ESI-mass spectrum (MeOH) of **1b**. The inset is the observed isotopic pattern (top) for the $[M - Cl - OH + H]^+$ peak compared to the simulated isotopic pattern (bottom).

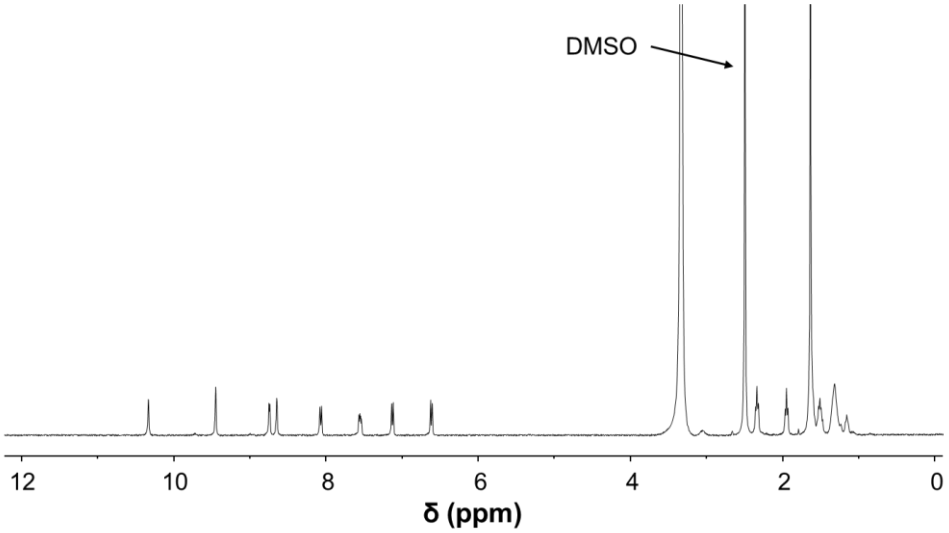

Figure S21. ^{1}H NMR spectrum of **1c** in DMSO-d_6.

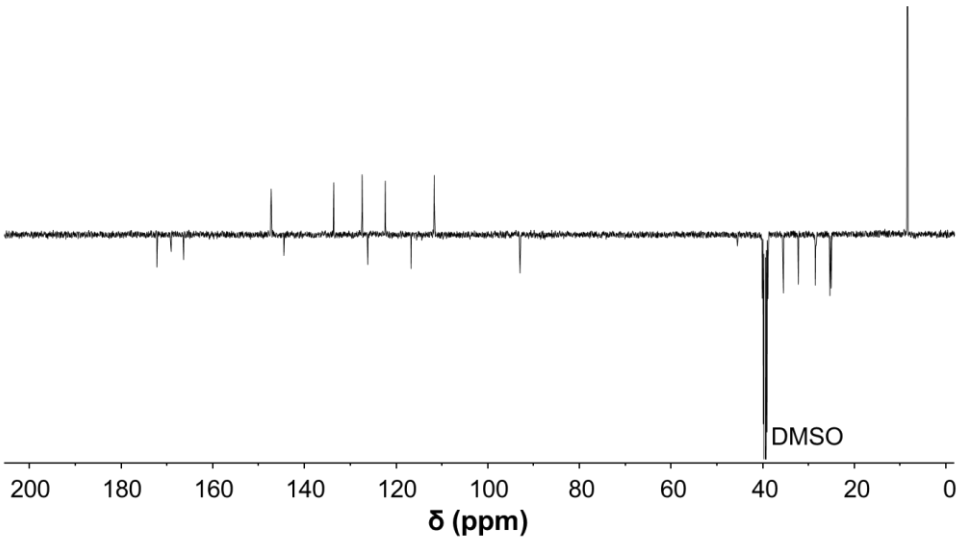

Figure S22. $^{13}C\{^{1}H\}$ DEPT-Q NMR spectrum of **1c** in DMSO-d_6.

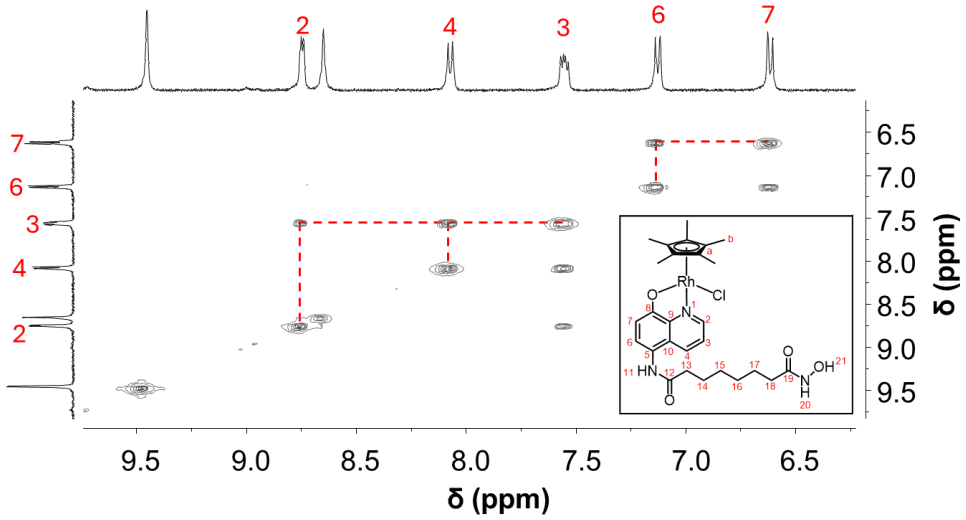

Figure S23. ^{1}H-^{1}H COSY NMR spectrum of **1c** in DMSO-d_6.

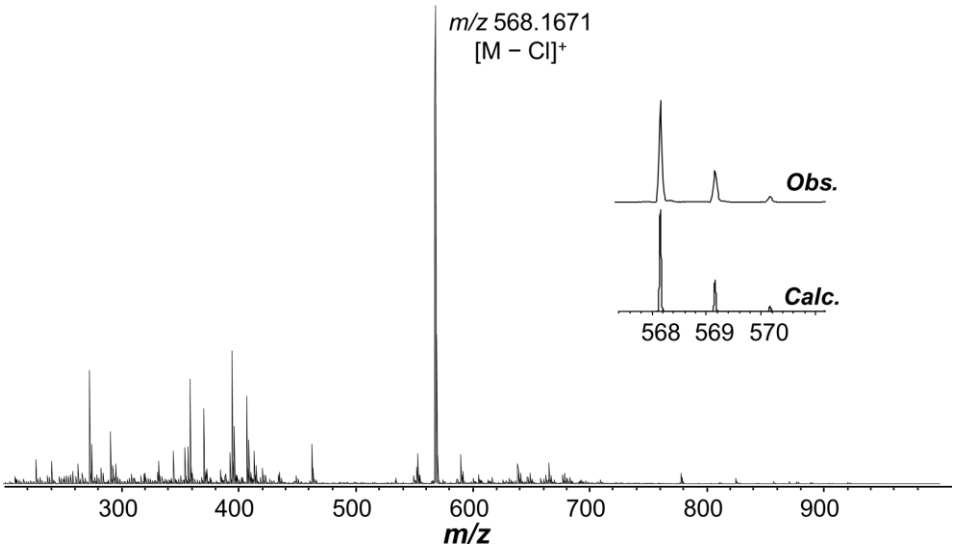

Figure S24. HR-ESI-mass spectrum (MeOH) of **1c**. The inset is the observed isotopic pattern (top) for the $[M - Cl]^+$ peak compared to the simulated isotopic pattern (bottom).

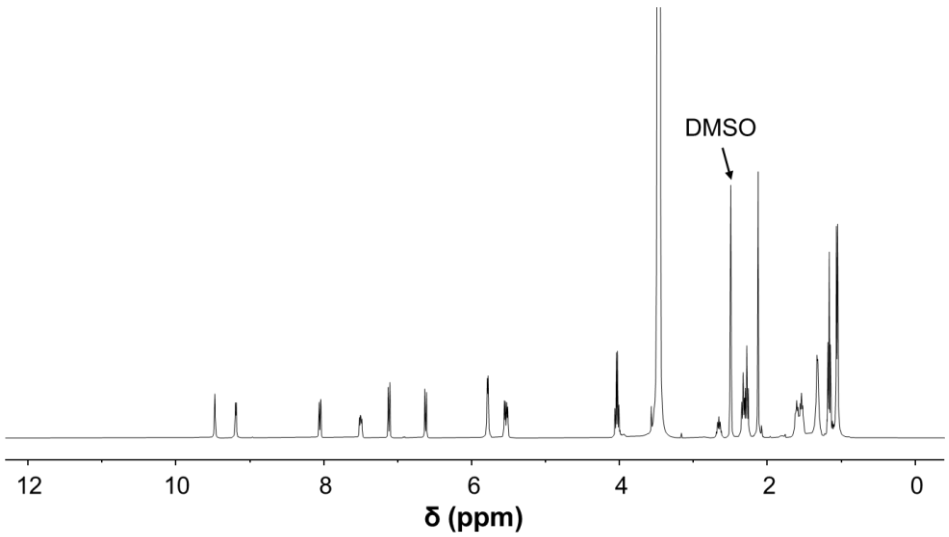

Figure S25. ^{1}H NMR spectrum of **2a** in DMSO-d_6.

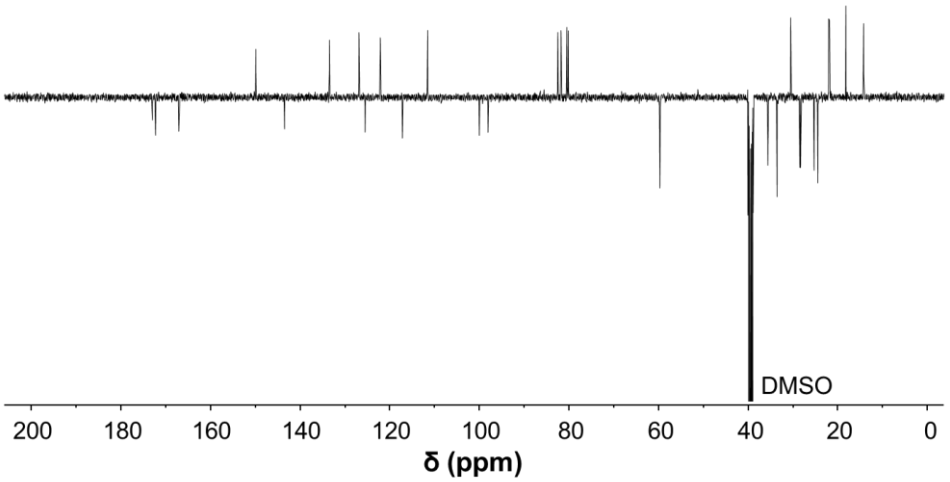

Figure S26. $^{13}C\{^{1}H\}$ DEPT-Q NMR spectrum of **2a** in DMSO-d_6.

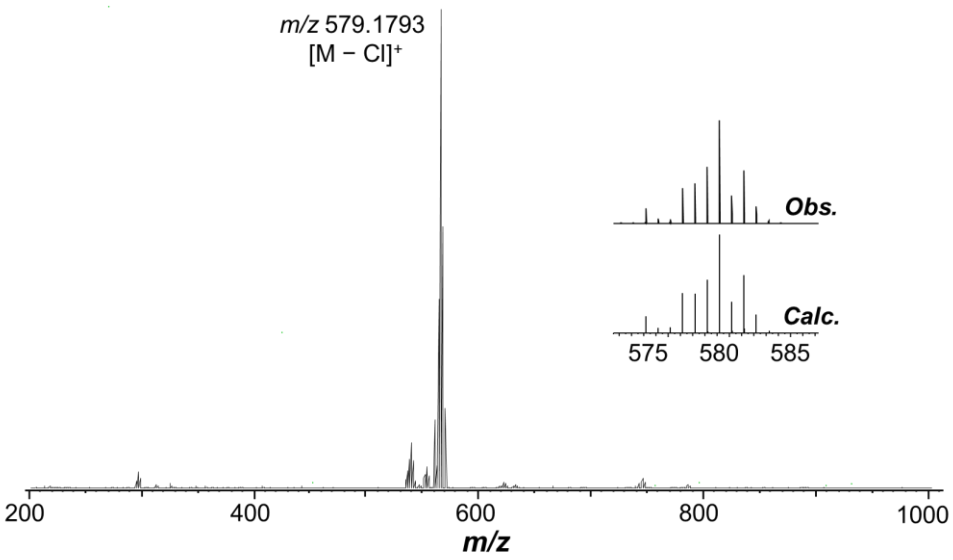

Figure S27. HR-ESI-mass spectrum (MeOH) of **2a**. The inset is the observed isotopic pattern (top) for the $[M - Cl]^+$ peak compared to the simulated isotopic pattern (bottom).

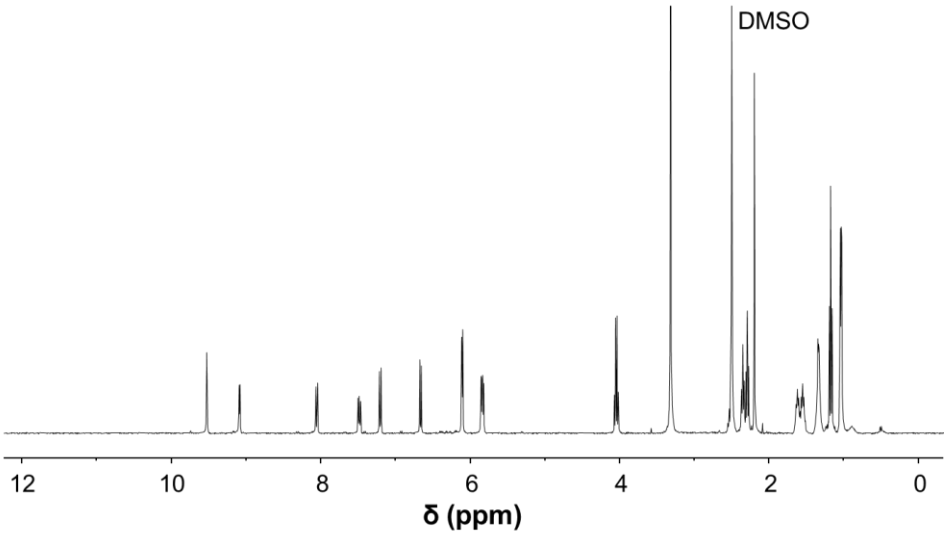

Figure S28. ^{1}H NMR spectrum of **2b** in DMSO-d_6.

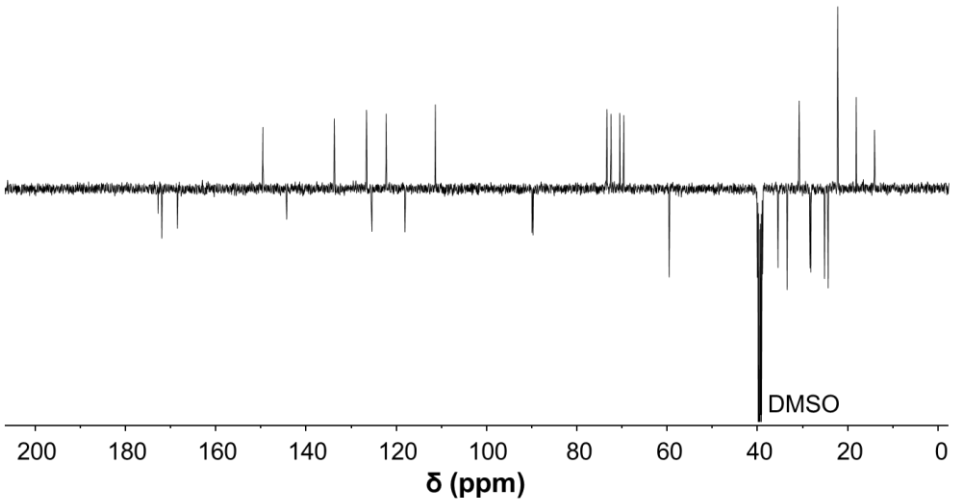

Figure S29. $^{13}C\{^{1}H\}$ DEPT-Q NMR spectrum of **2b** in DMSO-d_6.

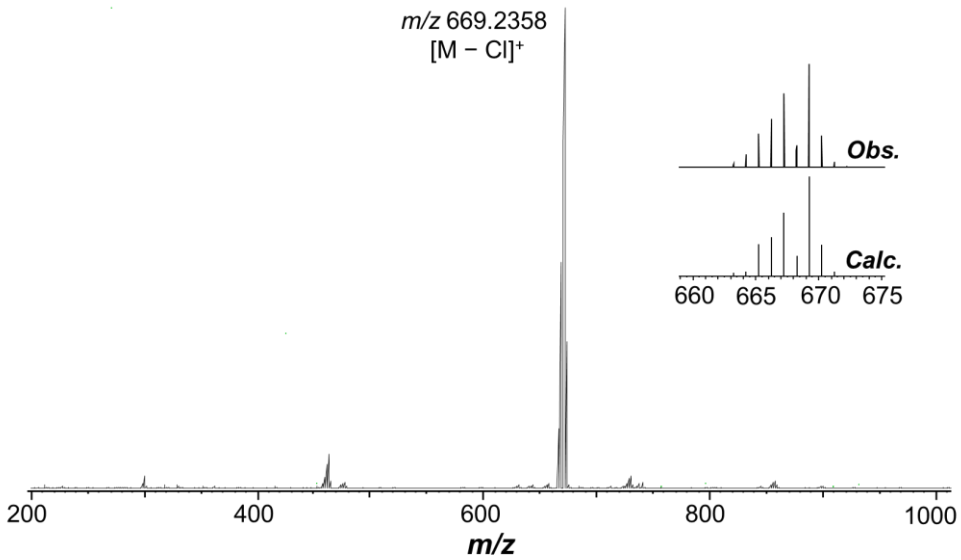

Figure S30. HR-ESI-mass spectrum (MeOH) of **2b**. The inset is the observed isotopic pattern (top) for the $[M - Cl]^+$ peak compared to the simulated isotopic pattern (bottom).

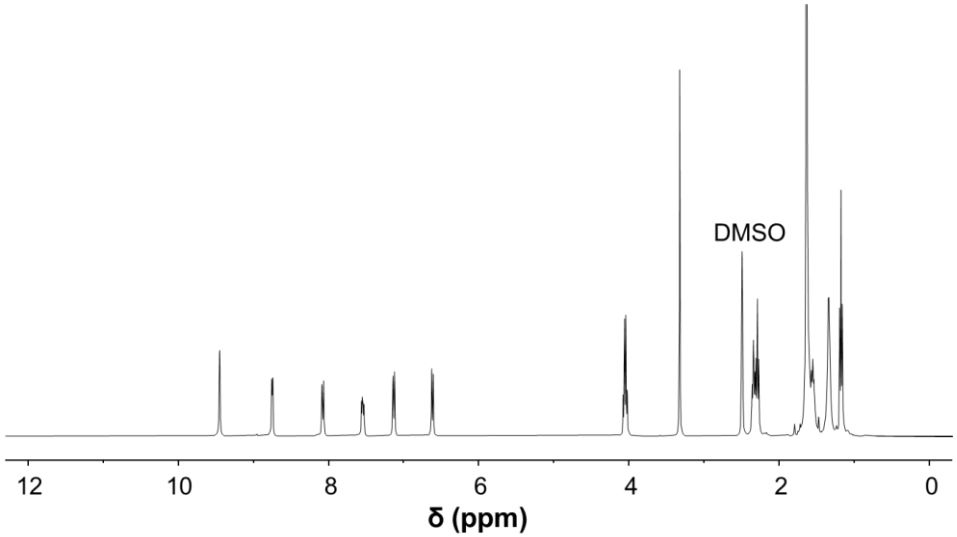

Figure S31. ^{1}H NMR spectrum of **2c** in DMSO-d_6.

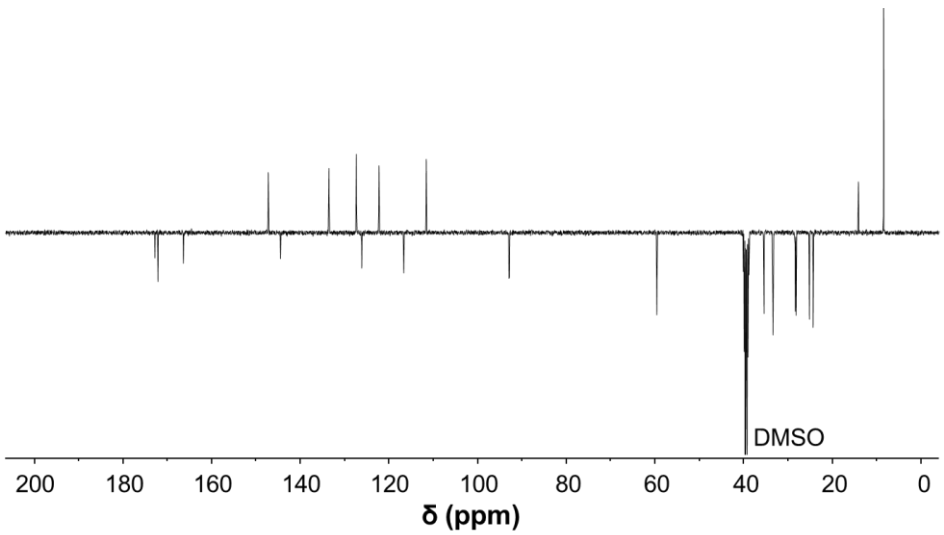

Figure S32. $^{13}C\{^{1}H\}$ DEPT-Q NMR spectrum of **2c** in DMSO-d_6.

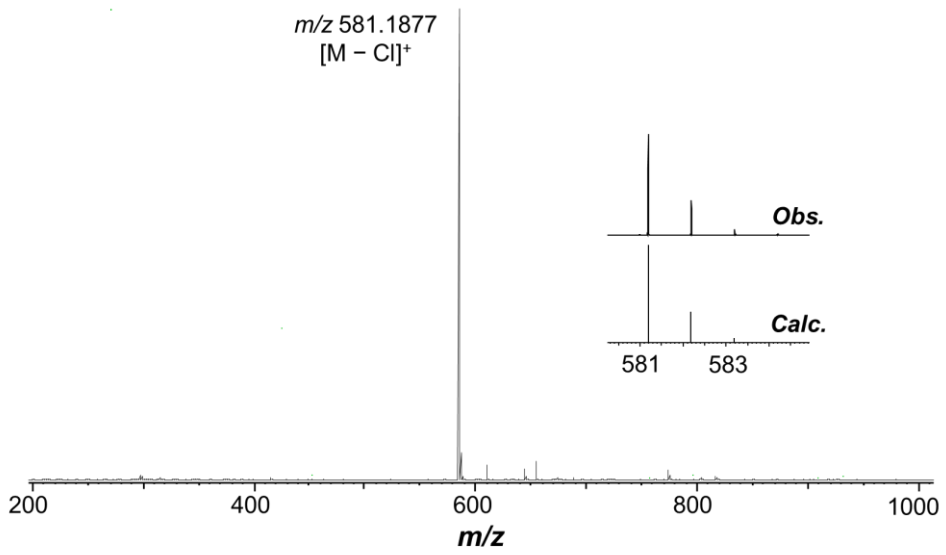

Figure S33. HR-ESI-mass spectrum (MeOH) of **2c**. The inset is the observed isotopic pattern (top) for the $[M - Cl]^+$ peak compared to the simulated isotopic pattern (bottom).

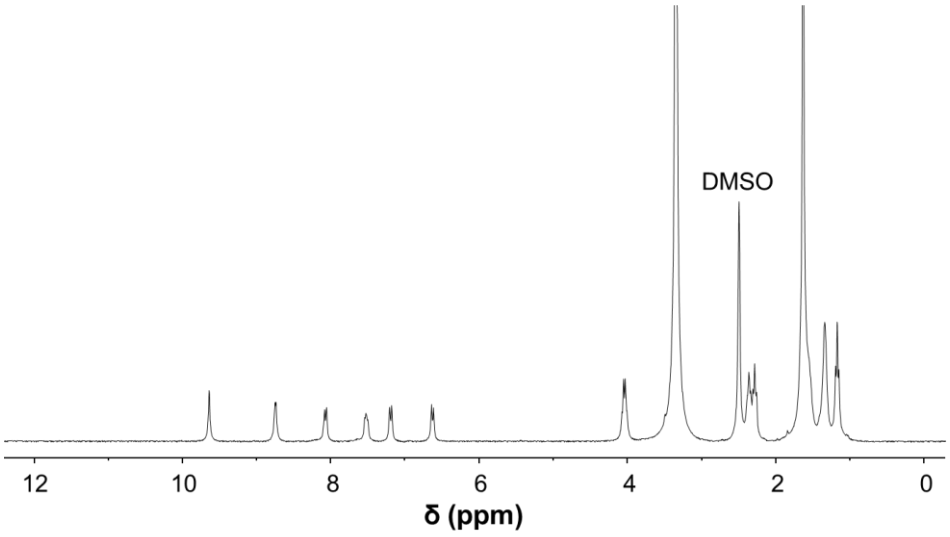

Figure S34. ^{1}H NMR spectrum of **2d** in DMSO-d_6.

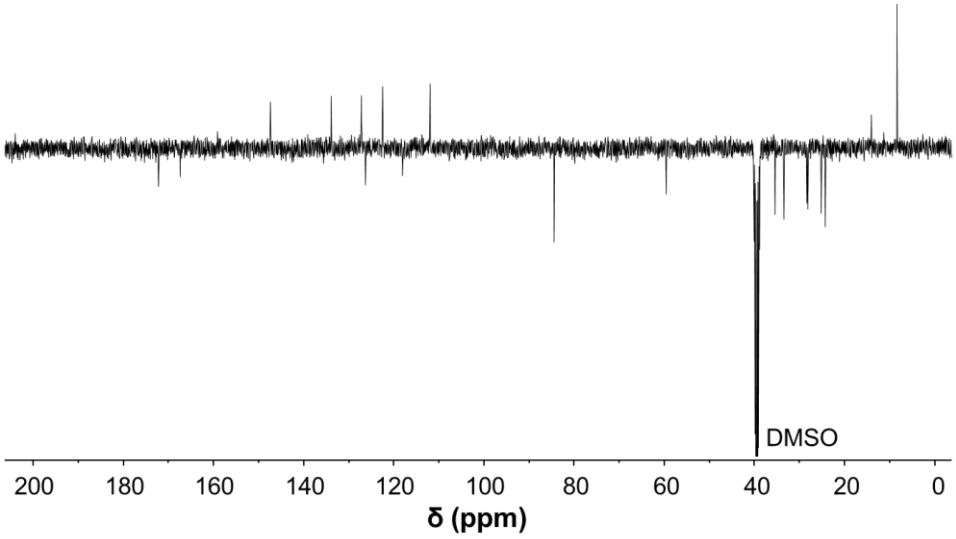

Figure S35. $^{13}C\{^{1}H\}$ DEPT-Q NMR spectrum of **2d** in DMSO-d_6.

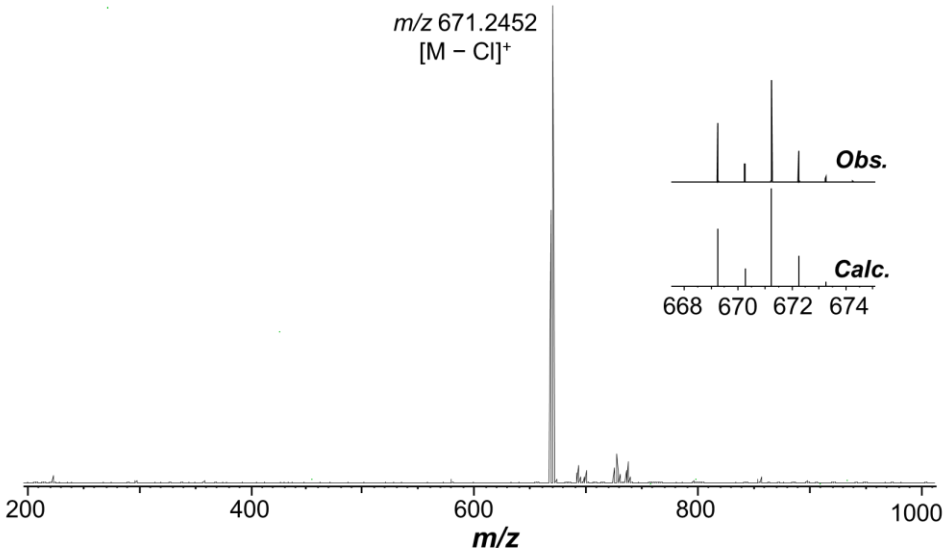

Figure S36. HR-ESI-mass spectrum (MeOH) of **2d**. The inset is the observed isotopic pattern (top) for the $[M - Cl]^+$ peak compared to the simulated isotopic pattern (bottom).

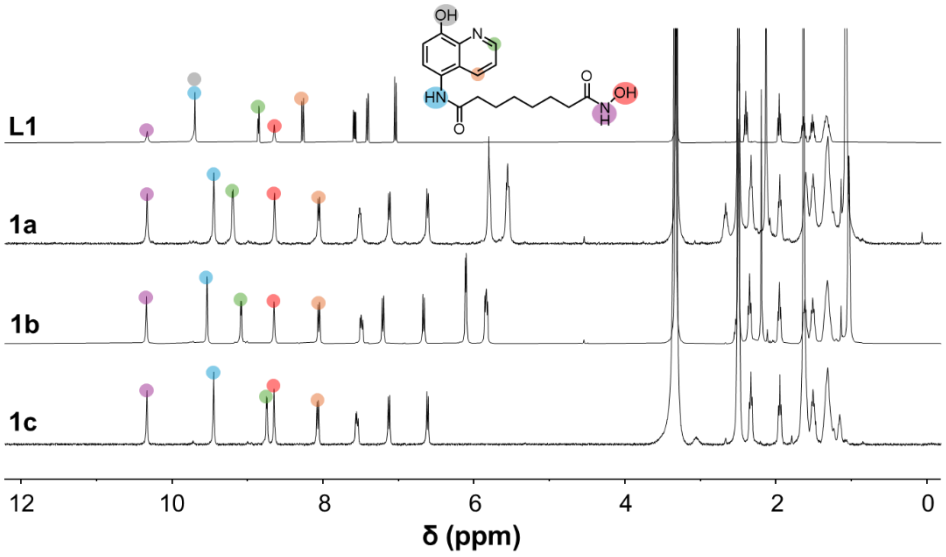

Figure S37. ^{1}H NMR spectrum of ligand **L1** in comparison to those of complexes **1a**–**1c** in DMSO-d_6. The coloured dots indicate the shifting observed upon coordination of **L1** to the metal centres.

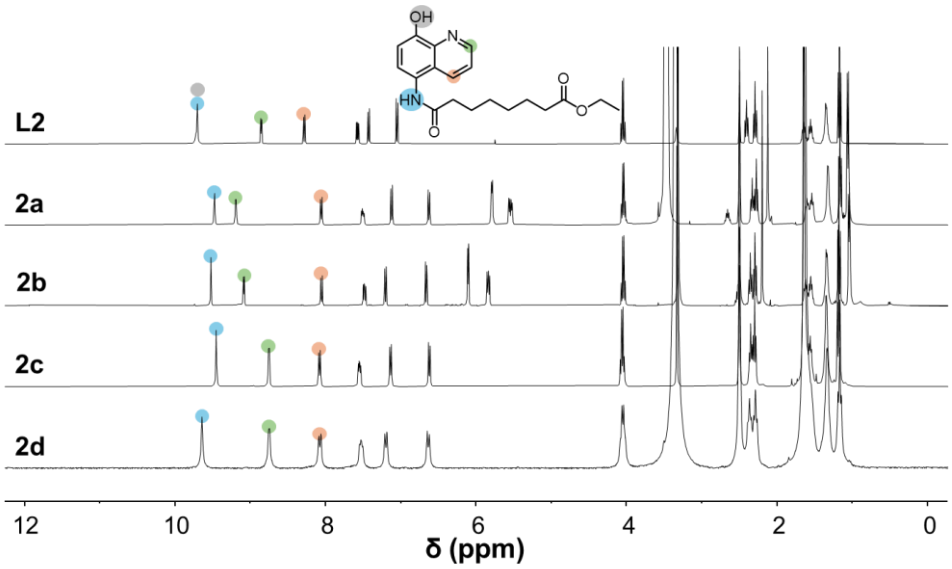

Figure S38. ^{1}H NMR spectrum of ligand **L2** in comparison to those of complexes **2a**–**2d** in DMSO-d_6. The coloured dots indicate the shifting observed upon coordination of **L2** to the metal centres.

Western blots

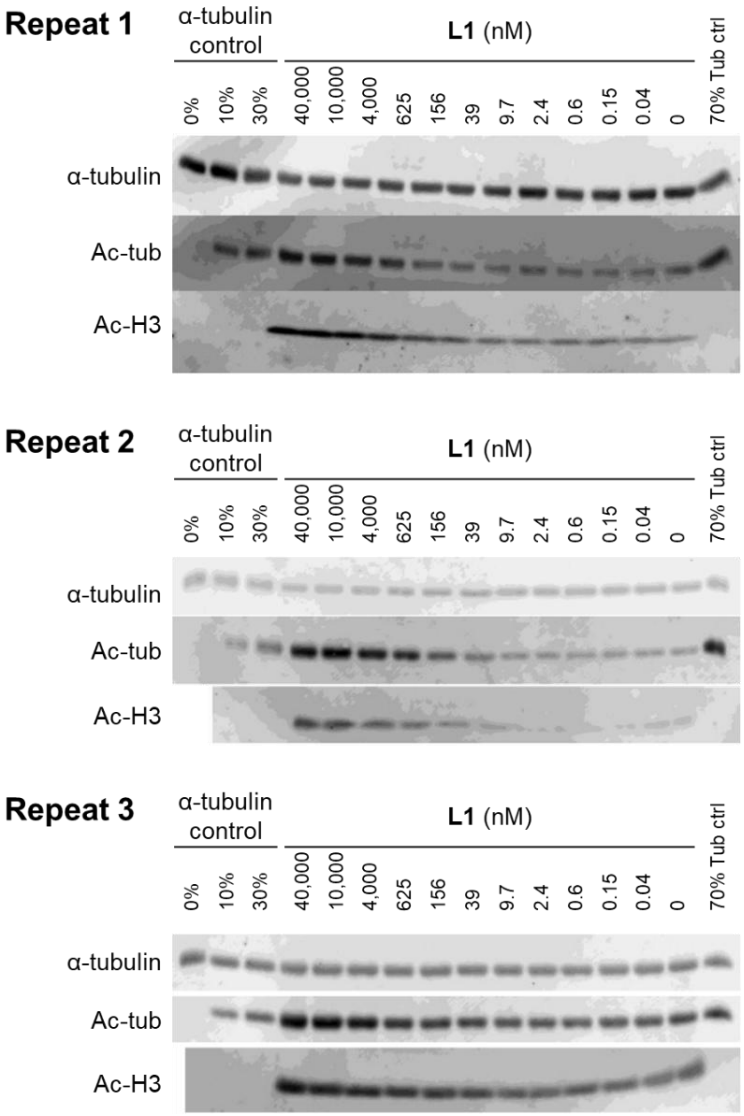

Figure S39. Western blots for **L1**.

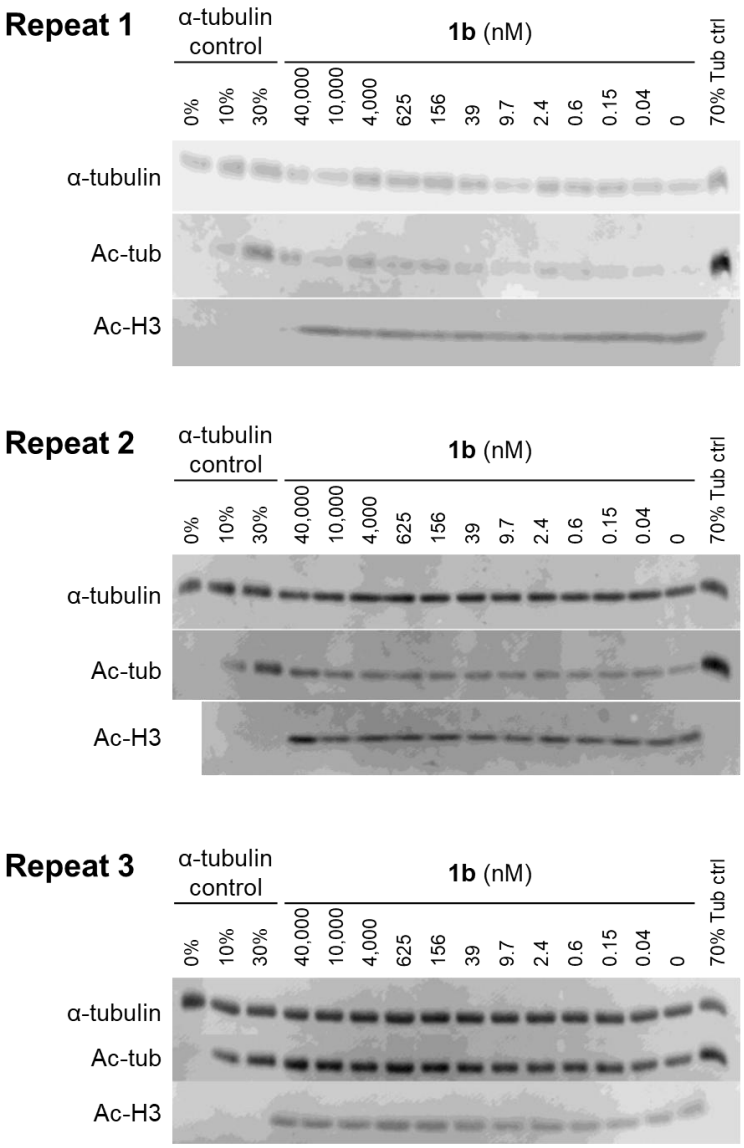

Figure S40. Western blots for **1b**.

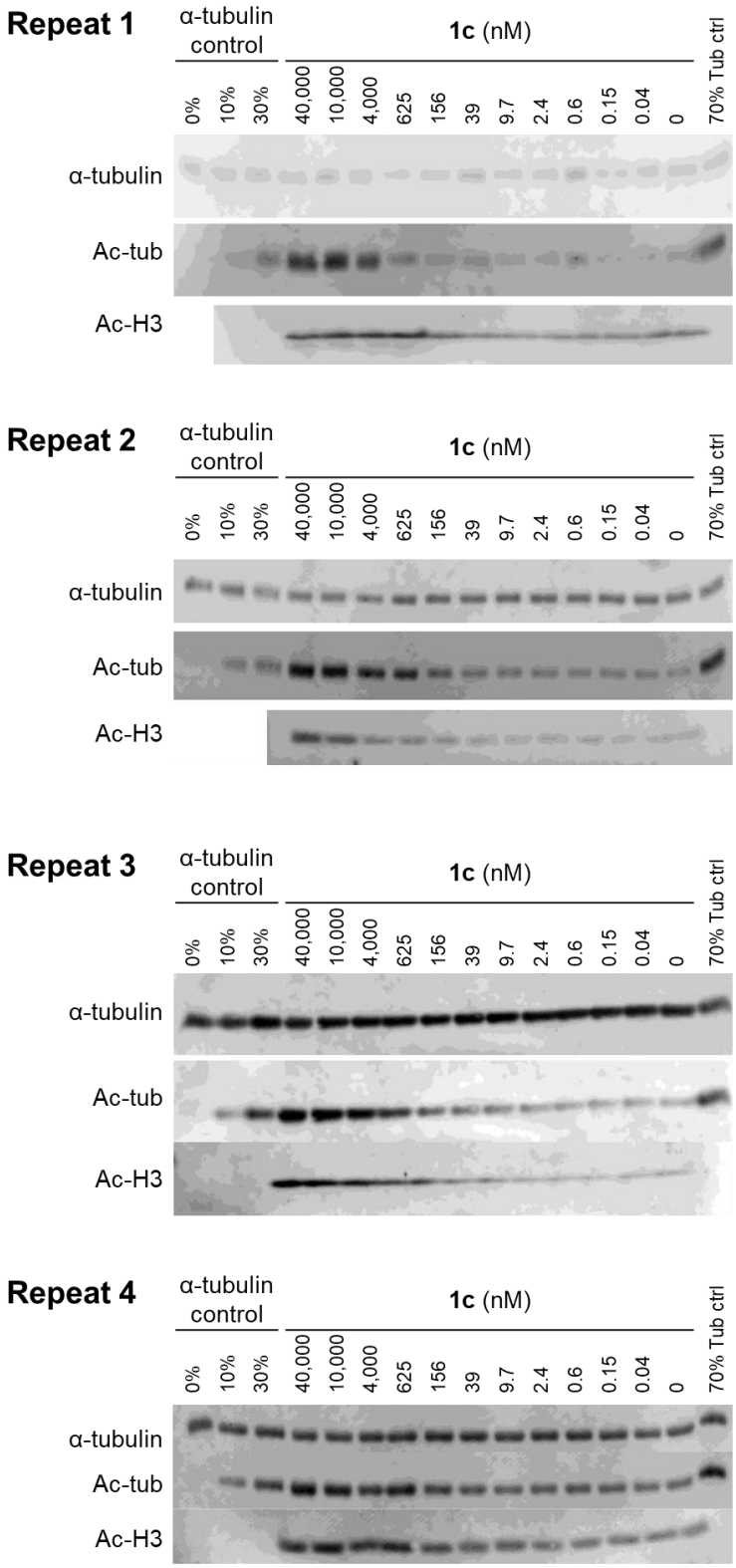

Figure S41. Western blots for **1c**.

References

1. C. Chen, X. Yang, H. Fang and X. Hou, Design, synthesis and preliminary bioactivity evaluations of 8-hydroxyquinoline derivatives as matrix metalloproteinase (MMP) inhibitors, *Eur. J. Med. Chem.*, 2019, **181**, 111563.
2. A. A. Grolla, V. Podestà, M. G. Chini, S. Di Micco, A. Vallario, A. A. Genazzani, P. L. Canonico, G. Bifulco, G. C. Tron, G. Sorba and T. Pirali, Synthesis, Biological Evaluation, and Molecular Docking of Ugi Products Containing a Zinc-Chelating Moiety as Novel Inhibitors of Histone Deacetylases, *J. Med. Chem.*, 2009, **52**, 2776–2785.
3. B. A. Chalmers, H. Xing, S. Houston, C. Clark, S. Ghassabian, A. Kuo, B. Cao, A. Reitsma, C.-E. P. Murray, J. E. Stok, G. M. Boyle, C. J. Pierce, S. W. Littler, D. A. Winkler, P. V. Bernhardt, C. Pasay, J. J. De Voss, J. McCarthy, P. G. Parsons, G. H. Walter, M. T. Smith, H. M. Cooper, S. K. Nilsson, J. Tsanaktsidis, G. P. Savage and C. M. Williams, Validating Eaton's Hypothesis: Cubane as a Benzene Bioisostere, *Angew. Chem., Int. Ed.*, 2016, **55**, 3580–3585.
4. C. O'Connor, D. C. Lawlor, C. Robinson, H. Müller-Bunz and A. D. Phillips, Comprehensive Experimental and Computational Study of η^6-Arene Ruthenium(II) and Osmium(II) Complexes Supported by Sulfur Analogues of the β-Diketiminate Ligand, *Organometallics*, 2018, **37**, 1860–1875.
5. P. Stoppioni, M. Divaira and P. M. Maitlis, Pentamethylcyclopentadienylrhodium Complexes with Tripod Tetradentate Ligands and Bidentate 'Mixed' Ligands, *J. Chem. Soc., Dalton Trans.*, 1982, **6**, 1147–1154.
6. B. A. Chalmers, H. Xing, S. Houston, C. Clark, S. Ghassabian, A. Kuo, B. Cao, A. Reitsma, C. E. Murray, J. E. Stok, G. M. Boyle, C. J. Pierce, S. W. Littler, D. A. Winkler, P. V. Bernhardt, C. Pasay, J. J. De Voss, J. McCarthy, P. G. Parsons, G. H. Walter, M. T. Smith, H. M. Cooper, S. K. Nilsson, J. Tsanaktsidis, G. P. Savage and C. M. Williams, Validating Eaton's Hypothesis: Cubane as a Benzene Bioisostere, *Angew. Chem., Int. Ed.*, 2016, **55**, 3580–3585.
7. J. Ptacek, I. Snajdr, J. Schimer, Z. Kutil, J. Mikesova, P. Baranova, B. Havlinova, W. Tueckmantel, P. Majer, A. Kozikowski and C. Barinka, Selectivity of Hydroxamate- and Difluoromethyloxadiazole-Based Inhibitors of Histone Deacetylase 6 In Vitro and in Cells, *Int. J. Mol. Sci.*, 2023, **24**, 4720.
8. J. Mikesova, M. Ondrakova, I. Jelinkova, J. Ptacek, Z. Novakova and C. Barinka, Determining Potency of Inhibitors Targeting Histone Deacetylase 6 by Quantification of Acetylated Tubulin in Cells, *Methods Mol. Biol.*, 2023, **2589**, 455–466.
9. M. Riisom, S. J. Morrow, C. D. Herbert, W. D. J. Tremlett, J. W. Astin, S. M. F. Jamieson and C. G. Hartinger, In vitro and in vivo accumulation of the anticancer Ru complexes [Ru^{II}(cym)(HQ)Cl] and [Ru^{II}(cym)(PCA)Cl]Cl, *J. Biol. Inorg. Chem.*, 2023, **28**, 767–775.

10. A. Daina, O. Michielin and V. Zoete, SwissADME: a free web tool to evaluate pharmacokinetics, drug-likeness and medicinal chemistry friendliness of small molecules, *Sci. Rep.*, 2017, **7**, 42717.
11. C. R. Groom, I. J. Bruno, M. P. Lightfoot and S. C. Ward, The Cambridge Structural Database, *Acta Crystallogr., Sect. B*, 2016, **72**, 171–179.
12. *Gaussian 09* Revision A.02, M. J. Frisch, G. W. Trucks, H. B. Schlegel, G. E. Scuseria, M. A. Robb, J. R. Cheeseman, G. Scalmani, V. Barone, G. A. Petersson, H. Nakatsuji, X. Li, M. Caricato, A. Marenich, J. Bloino, B. G. Janesko, R. Gomperts, B. Mennucci, H. P. Hratchian, J. V. Ortiz, A. F. Izmaylov, J. L. Sonnenberg, D. Williams-Young, F. Ding, F. Lipparini, F. Egidi, J. Goings, B. Peng, A. Petrone, T. Henderson, D. Ranasinghe, V. G. Zakrzewski, J. Gao, N. Rega, G. Zheng, W. Liang, M. Hada, M. Ehara, K. Toyota, R. Fukuda, J. Hasegawa, M. Ishida, T. Nakajima, Y. Honda, O. Kitao, H. Nakai, T. Vreven, K. Throssell, J. A. Montgomery Jr., J. E. Peralta, F. Ogliaro, M. Bearpark, J. J. Heyd, E. Brothers, K. N. Kudin, V. N. Staroverov, T. Keith, R. Kobayashi, J. Normand, K. Raghavachari, A. Rendell, J. C. Burant, S. S. Iyengar, J. Tomasi, M. Cossi, J. M. Millam, M. Klene, C. Adamo, R. Cammi, J. W. Ochterski, R. L. Martin, K. Morokuma, O. Farkas, J. B. Foresman and D. J. Fox, Gaussian, Inc., Wallingford CT, 2016.
13. J. P. Perdew, M. Ernzerhof and K. Burke, Rationale for mixing exact exchange with density functional approximations, *J. Chem. Phys.*, 1996, **105**, 9982–9985.
14. F. Weigend and R. Ahlrichs, Balanced basis sets of split valence, triple zeta valence and quadruple zeta valence quality for H to Rn: Design and assessment of accuracy, *Phys. Chem. Chem. Phys.*, 2005, **7**, 3297–3305.
15. S. Grimme, J. Antony, S. Ehrlich and H. Krieg, A consistent and accurate *ab initio* parametrization of density functional dispersion correction (DFT-D) for the 94 elements H-Pu, *J. Chem. Phys.*, 2010, **132**.
16. A. V. Marenich, C. J. Cramer and D. G. Truhlar, Universal Solvation Model Based on Solute Electron Density and on a Continuum Model of the Solvent Defined by the Bulk Dielectric Constant and Atomic Surface Tensions, *J. Phys. Chem. B*, 2009, **113**, 6378–6396.
17. H. M. Berman, J. Westbrook, Z. Feng, G. Gilliland, T. N. Bhat, H. Weissig, I. N. Shindyalov and P. E. Bourne, The Protein Data Bank, *Nucleic Acids Res.*, 2000, **28**, 235–242.
18. *The PyMOL Molecular Graphics System* 3.1.6.1, Schrödinger, LLC, 2025.
19. G. Jones, P. Willett, R. C. Glen, A. R. Leach and R. Taylor, Development and validation of a genetic algorithm for flexible docking, *J. Mol. Biol.*, 1997, **267**, 727–748.
20. G. Sciortino, J. Rodríguez-Guerra Pedregal, A. Lledós, E. Garribba and J.-D. Maréchal, Prediction of the interaction of metallic moieties with proteins: An update for protein-ligand docking techniques, *J. Comput. Chem.*, 2018, **39**, 42–51.

21. G. Ortore, F. D. Colo and A. Martinelli, Docking of Hydroxamic Acids into HDAC1 and HDAC8: A Rationalization of Activity Trends and Selectivities, *J. Chem. Inf. Model.*, 2009, **49**, 2774–2785.
22. *Discovery Studio Visualizer* v24.1.0.23298, BIOVIA, Dassault Systèmes, San Diego, 2024.